Thermal Performance of Heat and Water Recovery Systems: Role of Condensing Heat Exchanger Material

by

Negar Mohammadaliha

M.Sc., Sharif University of Technology, 2013

B.Sc., University of Guilan, 2009

Thesis Submitted in Partial Fulfillment of the
Requirements for the Degree of
Master of Applied Science

in the
School of Mechatronic Systems Engineering
Faculty of Applied Science

SIMON FRASER UNIVERSITY

Fall 2019

Approval

Name:	**Negar Mohammadaliha**
Degree:	**Master of Applied Science**
Title:	**Thermal Performance of Heat and Water Recovery Systems: Role of Condensing Heat Exchanger Material**
Examining Committee:	**Chair:** Dr. Mohammad Narimani Lecturer
	Dr. Majid Bahrami Senior Supervisor Professor
	Dr. Koroush Zanganeh Supervisor Senior research scientist/ group leader at NRCan/CanmetEnergy
	Dr. Erik Kjeang Internal Examiner Associate Professor
Date Defended/Approved:	September 11, 2019

Abstract

There is enormous potential for recovering a significant amount of latent heat at temperatures below 100°C from flue gas of combustion-based heating systems due to the presence of water vapor in their exhaust streams. However, condensation of acids along with water vapor in heat and water recovery systems makes a highly corrosive environment, which is a major challenge and a determining factor in selecting suitable materials for condensing heat exchangers. Despite the low cost and great corrosion-resistant properties of plastics, their relatively low thermal conductivities are not ideal for thermal management systems. it is still uncertain how significantly increasing thermal conductivity of the heat exchanger's material affects thermal performance of the heat recovery systems. The present study aims to shed light on the effect of the thermal conductivity of a condensing heat exchanger's material on the thermal performance of the unit. For this purpose, an analytical model is developed to predict the thermal performance of condensing heat exchangers, designed for recovering heat and water from wet flue gas. Further, to validate the model, a custom-designed condensing heat exchanger with replaceable tubes is designed in our lab and tested with 304 stainless-steel tubes and FEP plastic tubes under different inlet conditions. For the range of inlet conditions considered in this study, results show that there is a threshold for the thermal conductivity of the material, at which increasing the conductivity any further does not affect the condensation efficiency notably. It is worthy of note that this threshold, with respect to thermal conductivity of commonly used materials for such heat exchangers, has relatively low magnitude (e.g.~10-15 $W \cdot m^{-1} \cdot K^{-1}$ for stainless steel). This finding is significantly important as it unlocks the potential of using materials such as plastics and polymers with thermally conductive additives for latent heat recovery from flue gas.

Keywords: Heat and water recovery; wet flue gas; condensing heat exchanger; plastics and polymers; thermal conductivity; latent heat; corrosion.

To my love Mohammad and my dear family for their support and encouragement

Acknowledgements

I would like to express my deep gratitude towards many great people who made accomplishing this dissertation possible and enjoyable for me. My special thanks go to my senior supervisor at Simon Fraser University (SFU), Dr. Majid Bahrami, for his great support and guidance throughout my master's studies, as well as my colleagues and friends at the Laboratory for Alternative Energy Conversion (LAEC). I am especially grateful to Dr. Claire McCague, who gave me her full support throughout all phases of the project.

I gratefully acknowledge the financial support received from the Natural Sciences and Engineering Research Council of Canada (NSERC) through the College-University Idea to Innovation Grant "From Waste to Clean Food" (NSERC CU-I2I 501951), which made this whole enterprise possible.

Finally, I would like to express my gratitude to my family, who always supported me in all stages of my personal life and professional career, and, more importantly, to a very special person, my husband, for his continued love, support, and encouragement.

Table of Contents

List of Tables

List of Figures

List of Acronyms

HEX	Heat Exchanger
CHEX	Condensing Heat Exchanger
HWRU	Heat and Water Recovery Unit
FS	Full Scale
PFA	Perfluoroalkoxy
PTFE	Polytetrafluoroethylene
FEP	Fluorinated ethylene propylene

Nomenclature

T	Temperature (°C)
ω	Humidity ratio ($g_{H2O}/kg_{dry\text{-}air}$)
RH	Relative humidity (%)
A	Area (m^2)
Δx	Length of a unit cell (m)
R	Thermal resistance ($K \cdot W^{-1}$)
h	Convective heat transfer coefficient ($W \cdot m^{-2} \cdot K^{-1}$)
d	Dimeter (m)
f	Friction factor (-)
Pr	Prandtl number (-)
Re	Reynolds number (-)
Nu	Nusselt number (-)
k	Thermal conductivity ($W \cdot m^{-1} \cdot K^{-1}$)
λ	Thermal conductivity of the tube material ($W \cdot m^{-1} \cdot K^{-1}$)
$\dot{m}$	Mass flow rate ($kg \cdot s^{-1}$)
$\dot{Q}$	Heat transfer rate (W)
k_m	Mass transfer coefficient ($m \cdot s^{-1}$)
h_{fg}	Latent heat of vaporization ($J \cdot kg^{-1}$)
y	Mole fraction of water vapor (-)
M	Molecular mass (kg)
c_p	Specific heat ($J \cdot kg^{-1} \cdot K^{-1}$)
$Le_{H2O\text{-}g}$	Lewis number of water vapor in flue gas (-)
S	Tube pitch (m)
ΔP	Pressure drop (Pa)
WRE	Water recovery efficiency (-)
HRE	Heat recovery efficiency (-)
HR	Total heat recovery rate (W)
C'	Coefficient of discharge (orifice plate)
β	Diameter ratio (orifice plate)

ε	Expansion factor (orifice plate)
κ	Isentropic exponent (-)
ρ	Density ($\mathrm{kg.m^{-3}}$)
D	Diameter of the pipes connected to the orifice plate (m)

Subscripts

g	Flue gas
HTF	Heat transfer fluid
v	Vapor
in	Inlet
out	Outlet
i	Inner tube surface
o	Outer tube surface
int	Interface
tot	Total
bulk	Bulk
cond	Condensation
max	Maximum
L	longitudinal direction
T	Transverse direction
s	Tube surface
sat	Saturation

Executive Summary

Motivation

A significant portion of the total energy of industrial plants such as oil and gas, petrochemical, and power plants is released into the environment in the form of low-temperature thermal energy or low-grade waste heat, i.e. with temperature less than 175°C. The flue gas generated from the combustion of fossil fuels or biofuels in process heating equipment, such as boilers, furnaces, and ovens, is one of the main sources of low-grade waste heat. In Canada, industry accounts for 38% of total energy demand, while 30-40% of the input energy into industrial processes is discharged into the ambient as waste heat. This is a tremendous amount of thermal energy that a portion of it can be harvested and utilized in a variety of applications ranging from building air conditioning to greenhouses for food production. Therefore, waste heat recovery and utilization especially from low-grade sources will be beneficial for improving the energy efficiency and decreasing fossil fuels consumption, greenhouse gas emissions, as well as reducing the release of harmful chemicals into the ambient, which are directly linked to climate change and our environmental impact.

Since flue gas is the product of burning fossil fuels, it approximately contains 5-20 vol% water vapor depending on the fuel type. Although challenging, presence of water vapor in the flue gas composition of process heating equipment makes it possible to not only recover considerable amount of latent heat of vaporization at relatively low temperature (less than 100°C), along with the sensible heat of flue gas, but also harvest the water and reuse it in industrial applications. However, flue gas is highly corrosive as it may contain sulfur oxides (SOx), nitrogen oxides (NOx), Hydrogen fluoride (HF), and hydrogen chloride (HCl) based on the fuel's chemical composition. Therefore, corrosion is considered as one of the main challenges of heat and water recovery from flue gas due to the condensation of acids such as sulfuric acid (H_2SO_4), nitric acid (HNO_3), and hydrochloric acid (HCl) on the surface of heat exchangers used in the process. In addition to corrosion resistance, other factors including cost, fabrication, weight, fouling, and thermal properties should be considered in material selection for the condensing heat exchangers used in heat and water recovery units that form the core of this technology. Although materials such as synthetic graphite, stainless steel, and titanium have been proposed to be used as the material of heat exchangers working in corrosive environment,

the high cost of these materials make them poor candidates for this application, and one of the main reasons for low market penetration of this technology. Although plastics and polymers are among the promising candidates for such applications due to their great corrosion resistance properties, low cost, and light weight, their thermal conductivities are relatively low that impedes their thermal performance which in turn leads to larger sizes. Therefore, assessing the significance of material's thermal conductivity and its effect on the overall efficiency of heat and water recovery systems sheds light on the potential of using polymeric and plastic heat exchangers for this and other applications. To this end, this thesis is focused on investigating the potential usage of plastic and polymers as the material of condensing heat exchangers for heat and water recovery from flue gas or other wet exhaust streams.

Objectives

The main objective of this research is to investigate the significance of the thermal conductivity of heat exchangers' material in their efficiency for recovering heat and water from wet exhaust streams. This goal includes development and assessment of the performance of a proof-of-concept condensing heat exchanger made of fluorinated ethylene propylene (FEP) with enhanced thermal conductivity for heat and water recovery from flue gas, compared to the same condensing heat exchanger made of stainless steel.

Methodology

A systematic approach has been adopted to achieve the objective of this research. the following milestones have been set and executed:

- Developed an analytical model to predict heat and water recovery efficiency of condensing tube-bank heat exchangers under various inlet conditions. The model has been used to design heat exchangers for heat and water recovery systems;

- Designed and fabricated a custom-built test bed to study the effect of tubes' material on the efficiency of heat and water recovery from flue gas; the experimental data have been used to assess the accuracy of the model in

predicting the efficiency of condensing heat exchangers made of 304 stainless-steel tubes and FEP plastic tubes under various inlet conditions;

- Investigated the performance of a plastic condensing heat exchanger compared to a heat exchanger with the same design/dimensions made of stainless-steel, using the lab-scale experimental setup;

- Analytically investigated the effect of material's thermal conductivity on heat and water recovery efficiency of condensing tube-bank heat exchangers under different inlet conditions;

Contributions

The following highlights the main outcomes of this research:

- An analytical model is developed and verified with experimental data under various inlet conditions. The proposed model can predict the performance of condensing tube-bank heat exchangers. The present model is significantly fast, and it includes salient geometrical parameters, material properties, and operational parameters.

- It was unclear in the literature how significantly increasing thermal conductivity of the heat exchanger's material affects the thermal performance of heat and water recovery systems. This study aimed to address this issue. Increasing the thermal conductivity of plastics from a typical value of 0.2 $W \cdot m^{-1} \cdot K^{-1}$ to around 1-2 $W \cdot m^{-1} \cdot K^{-1}$ leads to a significant enhancement in the efficiency of heat and water recovery systems. However, any further increase in thermal conductivity after this threshold leads only to a marginal improvement. This is of great importance as it enables using plastics or polymeric heat exchangers with modestly improved thermal conductivity, achievable with today's off-the-shelf material, in heat and water recovery applications.

Research Road Map

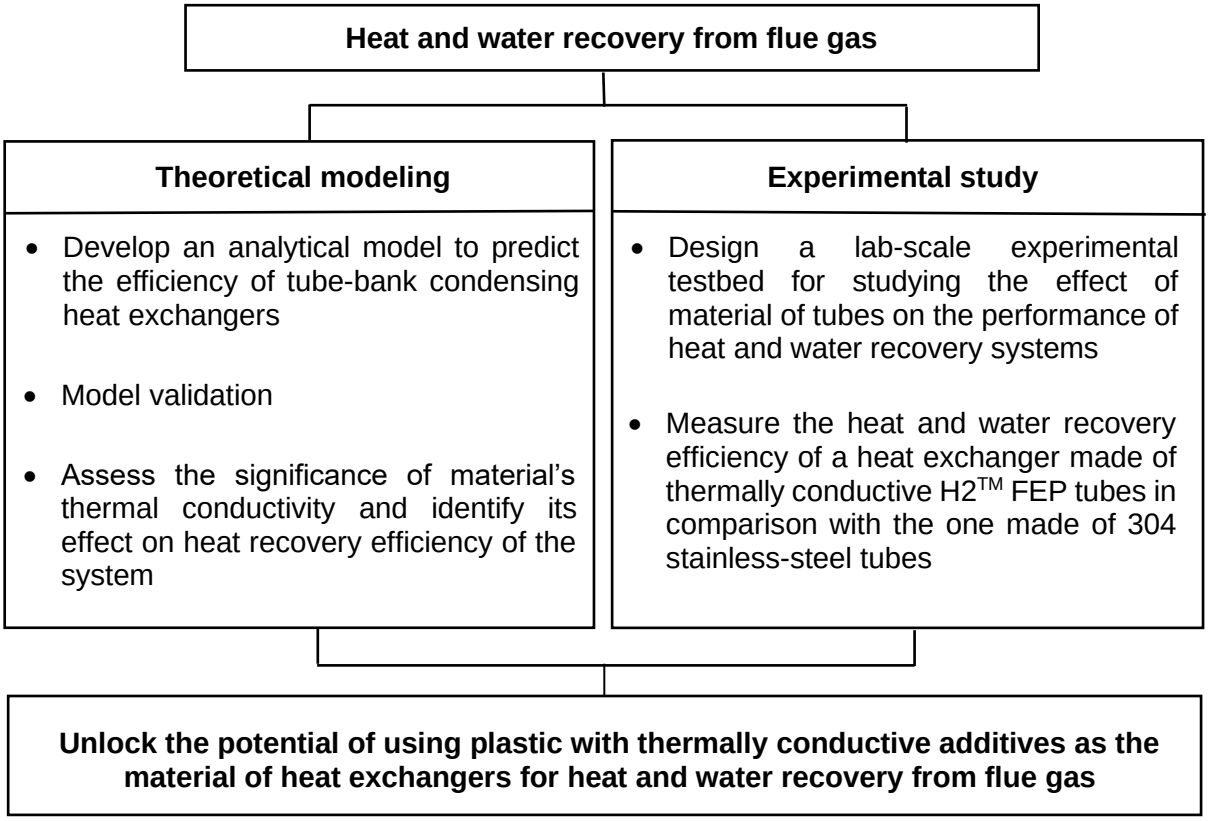

Chapter 1.

Introduction and literature review

1.1. Waste heat recovery

In the last few decades, climate change, global warming, and air pollution have raised global concerns over harmful environmental impacts of non-renewable energy systems. Considering that the global primary energy demand is predicted to increase by 33% by 2060 [1], enhancing the efficiency of non-renewable energy systems and replacing the fossil fuels by renewable energy resources have received a great deal of attention. The industry is one of the major consumers of energy in the world. As shown in Figure 1.1, in Canada, industry accounts for 38% of the total energy demand, while around 30-40% of the input energy into industrial processes is wasted [2], [3]. However, in China, the largest energy consumer in the world, the share of industrial sectors from the total energy consumption was even higher and around 62%, while around 50% of that energy was released to ambient as waste heat [4], [5]. The graphs, shown in Figure 1.1, highlight that significant portions of the annual energy demands of these countries are wasted to the ambient due to different sources of inefficiencies in industrial processes.

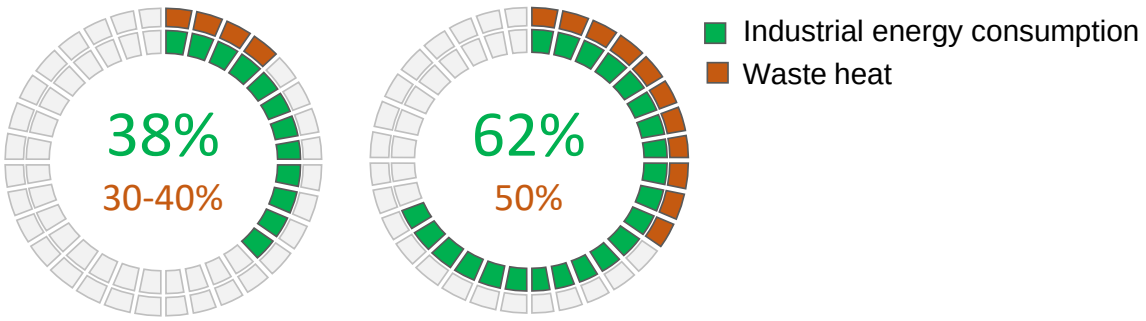

Figure 1.1. Share of energy consumptions of industrial sectors and their waste heat in total energy demand of (a) Canada and (b) China; circles represent the total annual energy demand of these countries.

Implementing waste heat recovery technologies by industrial sectors could lead to an enhancement in the energy efficiency of their processes by cutting the amount of their waste heat, which lowers their fossil fuel consumption and greenhouse gas emissions.

Flue gas, which is the hot gas discharged into the atmosphere via flues of process-heating equipment such as boilers, furnaces, and ovens, is one of the main sources of industrial waste heat. Although recovering the sensible heat of flue gas is a common practice in the industry, the capital and operational costs of heat recovery systems, the cost of energy, the size of the industrial plant, and the volume and schedule of operations significantly affect the long-term economic viability of using flue gas heat recovery technologies by industrial plants.

In a boiler, fossil fuels or biofuels are burned, and the boiler's water is heated using fuel's heat of combustion. As schematically shown in Figure 1.2, the efficiency of a conventional non-condensing boiler is usually around 75-77% while around 18% of the input energy is wasted into ambient from the flu-gas stack [6]. Economizers and air preheaters are commonly used by industrial sectors to recover the sensible heat of flue gas and reuse the recovered heat internally to increase the boiler efficiency by preheating the combustion air or boiler's feed water, respectively. The amount of sensible heat loss depends on the temperature and mass flow rate of the flue gas.

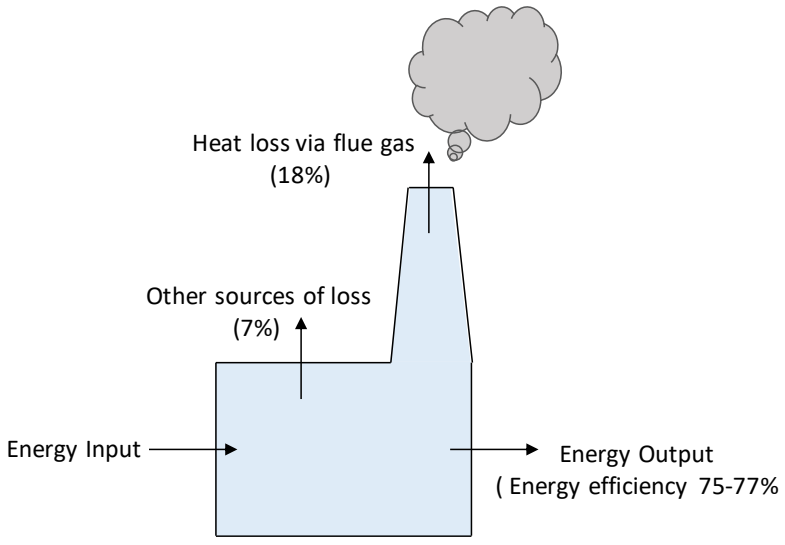

Figure 1.2. Energy balance in a non-condensing boiler.

Due to the presence of gas-state sulfric acid in the flue gas composition from burning fuels such as coal, bitument and heavy oil, the dew point of the sulfric acid is considered as the minimum temperature that flue gas can be cooled down without condensation of acids and consequent corrosion issue in heat recovery equipment and duct systems. The dew point temperature of the sulfuric acid in the flue gas depends on the pressure, the type of fuel burned in the boiler, sulfur content of the fuel, and excess air fraction [7]. Therefore, flue gas is discharged into the atmosphere at the temperature of around 90 -150˚C and is classified as low-grade waste heat. On the other hand, recovering low-grade waste heat is challenging since the efficiency of sensible heat transfer drops by decreasing the temperature of the hot source [8].

Fuel moisture, humidity of combustion air, and water vapor as a by-product of fuel oxidation, are three main sources of water vapor in the flue gas [9]. The volume concentration of water vapor in flue gas is 5-20% based on the type of boiler's fuel [9]. Due to the existence of water vapor in the flue gas, in conventional non-condensing boilers, the latent heat of vaporization of water vapor is also wasted into the ambient along with its sensible heat. Based on a report from Natural Resources Canada [6], the latent heat loss due to discharging of water vapor through the flue-gas stack is around 11% for natural gas and 7% for fuel oil. However, condensing boilers could reach efficiencies of even higher than 100% by having internal condensing heat exchangers (CHEXs), depending on their exit flue gas temperature and other working conditions [10]. Moreover, a non-condensing boiler can be retrofitted by externally adding a CHEX to further decrease the boiler's flue gas temperature and recover the latent heat of flue gas [11]. In this way, recovering latent heat along with sensible heat not only increase the efficiency of the heat recovery system, but also makes it possible to recover and reuse the water content of flue gas instead of discharging it into ambient. The increase in the fan power consumption due to adding CHEXs is insignificant compared to the energy saving that could be achieved [11]. It should be mentioned that the application of heat and water recovery units (HWRUs) is not limited to process heating equipment. Using this technology, heat and water recovery can be done on any wet exhaust streams like the exhaust of dryers. Qin et al. [12] investigated heat and water recovery from the exhaust of dryers with water vapor mass fraction of 5-28% using a tube-bank CHEX.

1.2. Benefits of Using HWRUs

Recovering sensible and latent heat from flue gas of combustion-based heating systems is the main advantage of implementing HWRUs. Szulc et al. [13] investigated the performance of a pilot-scale HWRU made of Teflon tubes in a lignite-fired power plant. The total heat recovery rate of the unit was reported around 312 kW, which 60% of it was the share of latent heat [13]. Xiong et al. [14] built and tested a plastic HWRU, and reported that 80% of the recovered heat came from recovering the latent heat while the share of sensible heat was only 20%, which clearly showed the significance of latent heat recovery. Jia et al. [15] showed that where the mass fraction of water vapor in the flue gas was higher than 8%, the share of sensible heat compared to the latent heat became insignificant and at some point negligible. The recovered heat by HWRUs can be utilized internally to enhances the efficiency of combustion-based heating systems and cutting the fuel consumption. For example, Hwang et al. [16] reported 5-10% enhancement in the efficiency of a gas-fired water heater using in-line and staggered tube-bank heat exchangers, made of crushed titanium tubes, for latent heat recovery. HWRUs can also be integrated into other systems such as space heating systems [17] and district heating networks [13], [18]. Using a theoretical model, Terhan and Comakli [18] showed that the domestic hot water of 184 flats could be supplied by integrating a waste heat recovery condenser into a 60 MW natural-gas fired district heating system, which was equivalent to 10.6% fuel saving. Their economic analysis showed that the payback period for this system was less than one year [18]. Zhao et al. [17] showed that the efficiency of the heat recovery process from a natural-gas fired boiler could be enhanced around 10 percent by implementing an absorption heat pump to further decrease the return temperature of the district heating systems and use it as the heat transfer fluid to cool down the flue gas.

Recovering water from flue gas is extremely beneficial, especially for regions with a shortage of water resources. Xiong et al. [19] showed that in case of 600-MW lignite-burned powerplant, 61.6 $t \cdot h^{-1}$ of water could be potentially recovered using an HWRU, which was enough to run the desulfurization unit with zero-net water consumption. Li et al. [20] showed that the recovered water from a 300 MW lignite-fired generator, using a flash evaporation and condensation device combined with a heat pump, was enough to run the flue gas desulfurization unit with zero-net water consumption. The HWRU built and tested by Xiong et al. [14] reached to the water recovery efficiency of up to 85 percent

[14]. Moreover, Jeong et al [21] built and tested an HWRU, consisting of six stainless-steel heat exchangers in series, with maximum water recovery efficiency of 70% within the range of inlet conditions considered in their study.

Biofuels are considered as potential alternatives to fossil fuels in combustion-based heating systems. However, high moisture content of biofuels deteriorates the efficiency of the heating system because of increasing the volume concentration of water vapor in the flue gas, which is discharged into the atmosphere in conventional economizers [22]. Dzurenda and Banski [23] showed that the energy content of flue gas of wood-fired boilers considerably increased by burning woods with higher moisture content. Therefore, the pre-drying process was recommended to decrease the moisture content of biofuels prior to using them as the fuel of combustion-based heating systems [24]. In this case, the sensible heat of flue gas can be recovered using conventional economizers and used as the input energy into the drying process. However, recovering the latent heat of water vapor using HWRUs can improve the efficiency of biofuels-fired heating systems and eliminate the drying process. Moreover, using fossil fuels with more hydrogen content and less carbon content leads to cleaner combustion. For example, burning natural gas release around 60% less CO_2 compared to coal [25]. Due to a higher hydrogen content of natural gas compared to coal and oil, flue gas emitted from burning natural gas contains higher concentration of water vapor to be recovered by HWRUs. Therefore, process heating equipment burning biofuels or fossil fuels such as natural gas can benefit most from implementing HWRUs.

In addition to main products of combustion such as CO_2 and H_2O, flue gas may contain sulfur oxides, (SOx), nitrogen oxides (NOx), Hydrogen fluoride (HF), and hydrogen chloride (HCl) based on the fuel's chemical composition [26]. There are some strict regulations on scrubbing the flue gas before discharging it into the atmosphere to prevent the formation of acid rains. Therefore, conventional and modern cleaning technologies are usually used by industry to meet the emission limits. Besides heat and water recovery from flue gas, cutting toxic and harmful emissions to some extent is one of the side advantages of using HWRUs. Jia et al. [27] observed a 20-40% SO_2 scrubbing rate depending on the flue gas temperature and vapor concentration. Moreover, the mercury concentration in flue gas of a coal-fired power plant decreased by 60% using an HWRU [28].

1.3. Challenges of implementing HWRUs

Fouling is considered as one of the main operational problems of heat exchangers. Although simultaneous mechanisms cause fouling in a heat exchanger, particulate fouling is the dominant type of fouling in an HWRU due to the presence of ash and solid particles in the flue gas [29]. As a result of particulate fouling, deposition of solid particles and dirt on the surfaces of a heat exchanger causes an additional undesired thermal resistance which can significantly deteriorate the heat transfer performance and add cleaning costs. Lie et al. [30] studied the fouling of a condensing finned tube bundle for different sizes of ash and lignite particles in the flue gas. The issue of fouling is out of the scope of this study and more information about the fouling of heat exchangers working in flue gas heat recovery systems can be found in the literature [29].

Results of a comprehensive study done by Levy et al. [28] showed that sulfuric acid (H_2SO_4), hydrochloric acid (HCl), and nitric acid (HNO_3) condensed in HWRUs along with water vapor. Condensation of acids in HWRUs makes a highly corrosive environment and makes the corrosion a major challenge and a determining factor in selecting suitable materials for CHEXs. Levy et al. [28] performed long-term corrosion tests on a wide range of materials, including steels, stainless steels, nickel alloys, aluminium, polymers, and graphite, under different temperatures and sulfuric acid concentrations. Results of this study showed that Nickel alloys 22 and 690, as well as polymers such as FEP and polytetrafluoroethylene (PTFE), were suitable for corrosive environments, even with high concentrations of sulfuric acid [28]. Moreover, Xiong et al. [14] reported a self-cleaning capacity for the tube-bank heat exchanger made of perfluoroalkoxy (PFA), which they tested, due to presence of the condensate film on the tubes and vibration of tubes during the operation. Hwang et al. [16] tested a tube-bank heat exchanger made of crushed titanium tubes as an HWRU and observed no sign of corrosion or thermal performance drop after one year. Although most of the studies in the literature focused on using indirect condensing heat exchangers, Li et al. [20] proposed using cooling scrubber for recovering heat and water from flue gas to avoid the issues of fouling and corrosion. They used a heat pump to lower the cooling temperature of the flue gas and a flash evaporator to clean the recovered water which was mixed with slurry in the cooling scrubber [20]. Hong et al. [31] proposed a combination of using a CHEX and water spray to enhance the heat recovery performance. They showed that depending on the size of CHEXs, the heat

recovery rate enhanced by 1.3 - 2.2 times and pressure drop slightly increased compared to the case without spraying water.

The cost of implementing latent heat recovery systems not only includes the cost of components such as heat exchangers, piping and valves, but also installation, operational, and maintanace costs. In an economical analysis, Che et al. [11] showed that the material cost of heat exchangers was the main cost of implementing heat and water recovery systems.

1.4. Overview of HWRUs in the literature

The focus of this study is on using CHEXs for recovering heat and water from flue gas. Tube-bank CHEXs with in-line and staggered tube arrangement have been commonly used for this purpose in the literature [9], [14], [16], [21], [30]–[32]. Hwang et al. [16] showed that a CHEX with staggered tube arrangement had around two times higher convective heat transfer coefficient and pressure drop on the gas side compared to the one with the inline arrangement of tubes [16]. Types and materials of CHEXs, designed and tested in the literature for heat and water recovery from flue gas, are listed in Table 1.1. While most of the studies used stainless-steel heat exchangers for this purpose, Xiong et al. [14] and Jia et al. [27] studied the performance of plastic heat exchangers for this application. Jia et al. [27] designed and tested a spiral plate heat exchanger made of PTFE to recover sensible and latent heat from flue gas of a natural gas-fired boiler, where the share of latent heat recovery was 3 to 4 times of sensible heat transfer. Xiong et al. [14] also investigated the performance of a tube-bank heat exchanger made of fluorine plastic with the in-line arrangement of tubes for heat and water recovery from flue gas, motivated by the material's corrosion resistance.

Although plastics and polymers have low cost and great corrosion-resistant properties, their relatively low thermal conductivities are not ideal for thermal management systems. However, it is still uncertain how significantly the relatively low thermal conductivities of plastics affect the thermal performance of HWRUs. Since the performance parameters of an HWRU depend on the size and compactness of their CHEXs, it is challenging to compare the performance of stainless-steel CHEXs with plastic ones based on the data available in the literature. This study aims to investigate how the thermal conductivity of a CHEX's material affects the heat and water recovery

performance of an HWRU. Results of this study show the potential of using plastic CHEXs instead of more expensive metallic heat exchangers such as ones made of stainless steel and titanium to reduce the cost of HWRUs.

Table 1.1. Types and materials of heat exchangers used for heat and water recovery from flue gas in the literature.

Ref.	Heat exchanger type	Heat exchanger material
[9], [21]	In-line tube-bank HEXs	Stainless steel
[15]	A vertical tube with cooling jacket	Stainless Steel
[31]	Tube-bank HEXs	Stainless steel
[33]	Compact fin-and-tube HEXs	SUS304
[32]	Staggered tube-bank HEXs	SUS304
[30]	Finned tube bank HEXs	Stainless steel
[16]	Staggered and in-line tube-bank HEXs	Titanium
[34]	Spiral tube HEXs	Copper
[13]	Shell-and-tube HEXs	Teflon
[14]	In-line tube-bank HEXs	PFA
[35]	Spiral plate HEXs	PTFE

Chapter 2.

Modeling the performance of tube-bank CHEXs for heat and water recovery from flue gas

A theoretical model has been developed to investigate the thermal performance of a CHEX composed of an in-line array of circular tubes. The geometrical parameters of the CHEX, its inlet conditions, and the thermal properties of the CHEX's material are the inputs of this model. The model predicts the outlet conditions as well as the performance parameters, including the total heat recovery rate, water recovery rate, heat recovery efficiency, and water recovery efficiency as the outputs (See Figure 2.1). Jeong et al. [20] and Terhan and Comakli [17] implemented the same approach to model flue gas condensation in heat and water recovery systems.

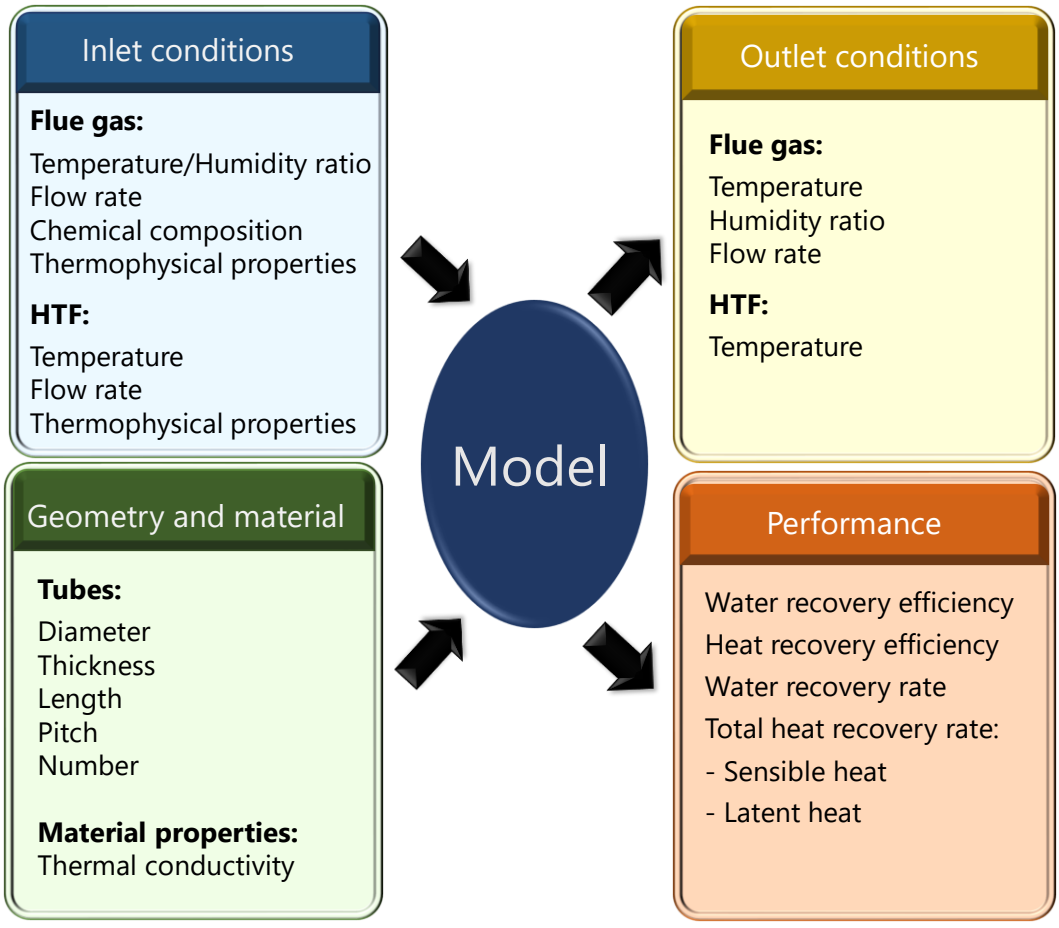

Figure 2.1. Inputs and outputs of the model.

2.1. Modeling Approach

This model considers a CHEX, which is a tube-bank HEX with in-line configuration of tubes, as a group of geometrical unit cells in form of short straight tube segments. This unit-cell approach has been successfully adopted by Navarro and Cabezas-Gomez to model the performance of single-phase air-to-liquid crossflow HEX [36], which is extended in our study to account for condensation in presence of non-condensable gasses. A unit cell of a tube-bank HEX is in the form of a tube segment with a length of Δx, which is shown schematically in Figure 2-2. The heat transfer fluid (HTF) and flue gas flow inside and outside of the tube, respectively. In the case of condensation, a layer of condensate is formed on the outer surface of the tube.

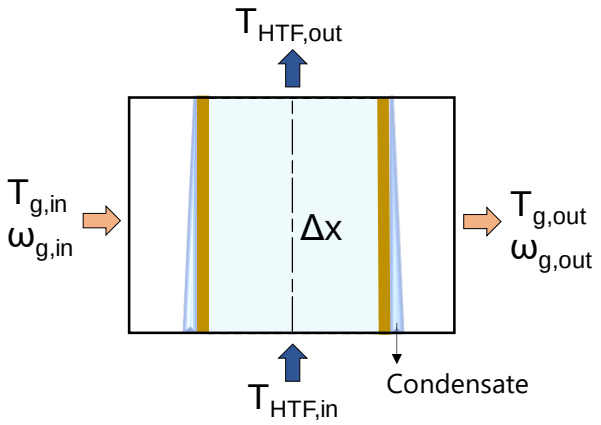

Figure 2-2. Condensation of wet flue gas in a unit cell of a tube-bank CHEX.

It is assumed that evaporation doesn't happen inside the tubes and the HTF remains single phase. For a unit cell, having the inlet conditions including the HTF temperature ($T_{HTF,in}$), the flue gas temperature ($T_{g,in}$), as well as humidity ratio of the flue gas ($\omega_{g,in}$) as the input parameters and solving the governing equations result in calculating the outlet conditions including the HTF temperature ($T_{HTF,out}$), the flue gas temperature ($T_{g,out}$), as well as the humidity ratio of the flue gas ($\omega_{g,out}$).

Two cases can be considered for the thermal resistance network of the unit cell shown in Figure 2-2. When the interface temperature is higher than the dew point temperature of the flue gas, only sensible heat transfer occurs between the HTF flow and the flue gas flow. In this case, the thermal resistance network is shown in Figure 2.3 a. However, when the tube surface temperature decreases below the dew point temperature of the flue gas, the water vapor in the flue gas starts to condense on the tube surface. In

this case, as shown in Figure 2.3 b, both sensible and latent heat is transferred to the HTF flow. Zhang et al. [37] showed that when the mass fraction of water vapor is less than 70%, the effect of conductive thermal resistance of the liquid condensate layer is negligible. Therefore, the thermal resistance of the condensate layer is neglected in the present model, and the temperature of the outer tube surface is considered the same as the interface temperature, denoted by T_{int}, which is the temperature of interface between flue gas and the condensate layer (see Figure 2.3 b).

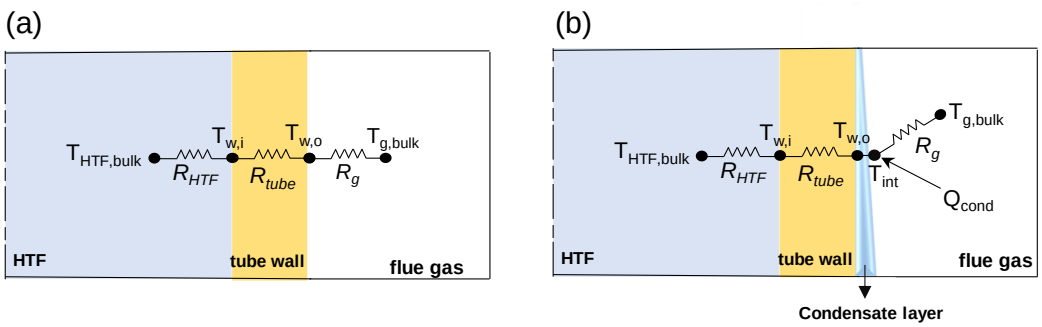

Figure 2.3. Thermal resistance networks of a unit cell a) in the absence of condensation and b) in the presence of condensation.

In the thermal resistance networks (see Figure 2.3), the convective thermal resistance from the bulk of flue gas and HTF to the tube wall, denoted by R_{HTF} and R_g, respectively, are defined as:

$$R_{HTF} = \frac{1}{h_{HTF} A_i} \tag{2.1}$$

$$R_g = \frac{1}{h_g A_o} \tag{2.2}$$

where, A_i and A_o are the inner and outer surface area of the tube segment, respectively. The HTF convective heat transfer coefficient, denoted by h_{HTF} in Eq. (2.1), is calculated based on the correlation provided by Gnielinski [38] (see Eq. (2.3)). This correlation is valid for transient and turbulent flows in a circular tube and its accuracy is more than 90% [39].

$$Nu_{HTF} = \frac{h_{HTF} d_i}{k_{HTF}} = \frac{\left(\frac{f}{8}\right)(Re_{HTF} - 1000)Pr}{1 + 12.7(f/8)^{1/2}(Pr^{2/3} - 1)} \quad (2.3)$$

$$[\,3000 \leq Re_{HTF} \leq 5 \times 10^6 \; and \; 0.5 < Pr < 2000]$$

where *f* is the friction factor that can be obtained from Moody diagram [39]. In general, friction factor depends on the Reynolds number and the relative roughness of tubes. In case of smooth tubes, *f* can be calculated as:

$$\mathrm{f} = (0.79\mathrm{Ln}(\mathrm{Re}_{HTF}) - 1.64)^{-2} \quad (2.4)$$

The convective heat transfer coefficient of flue gas flow, denoted by h_g in Eq. (2.2), is calculated based on the correlations provided by Zukauskas [40] for in-line tube arrangements (see Eq. (2.5) and (2.6)). It should be mentioned that at low Reynolds numbers, the convective heat transfer coefficient of the gas flowing through a tube bank is the same as a single tube (Eq. (2.6)). The Reynolds number ($Re_{g,max}$) for this correlations is calculated based on the outer tube diameter (d_o) and maximum velocity of the flue gas flowing through the tubes.

$$\overline{\mathrm{Nu}_g} = \frac{h_g d_o}{k_g} = 0.27\mathrm{Re}_{g,\max}^{0.63}\mathrm{Pr}^{0.36}(\mathrm{Pr}/\mathrm{Pr}_s)^{\frac{1}{4}} \quad (2.5)$$

$$[1000 \leq Re_{g,max} \leq 2 \times 10^5 \; and \;\; 0.7 < \mathrm{Pr} < 500]$$

$$\overline{\mathrm{Nu}_g} = \frac{h_g d_o}{k_g} = 0.51\mathrm{Re}_{g,\max}^{0.63}\mathrm{Pr}^{0.5}(\mathrm{Pr}/\mathrm{Pr}_s)^{\frac{1}{4}} \quad (2.6)$$

$$[100 \leq Re_{g,max} \leq 1000 \; and \;\; 0.7 < \mathrm{Pr} < 500]$$

The thermal resistance of the tube wall, denoted by R_{tube}, is defined as:

$$R_{tube} = \frac{Ln(d_o/d_i)}{2\pi\lambda\Delta x} \quad (2.7)$$

where, λ represents the thermal conductivity of the tube material and d_i and d_o represent the inner and outer tube diameters, respectively. Considering the thermal resistance of the tube wall, there is a temperature difference between the inner and outer tube surfaces.

The energy balance on the interface of the condensate layer and the gas should be solved for the tube segment based on the thermal resistance networks. In the absence of condensation, the energy balance is expressed as:

$$(T_{g,bulk} - T_{w,o})/R_g = (T_{w,o} - T_{HTF,bulk})/(R_{tube} + R_{HTF}) \quad (2.8)$$

However, in the presence of condensation, the energy balance is written as:

$$\dot{Q}_{cond} + (T_{g,bulk} - T_{int})/R_g = (T_{int} - T_{HTF,bulk})/(R_{tube} + R_{HTF}) \quad (2.9)$$

where, the condensation heat flow, denoted by $\dot{Q}_{\mathrm{cond}}$, is calculated by Eq. (2.10).

$$\dot{Q}_{cond} = k_m A_o h_{fg} (y_{bulk,g} - y_{int}) \quad (2.10)$$

where k_m is the convective mass transfer coefficient, h_{fg} is the latent heat of vaporization of water vapor and $y_{bulk,g}$ and y_{int} are the mole fraction of water vapor in the bulk of gas and on the interface, respectively. It should be mentioned that $y_{bulk,g}$ is calculated based on the inlet humidity ratio of the flue gas using Eq. (2.11).

$$y_{bulk,g} = \frac{M_g \omega_g}{M_{H_2O}(\omega_g + 1)} \quad (2.11)$$

where M_{H2O} and M_g are the molecular mass of water vapor and flue gas, respectively. Moreover, y_{int} is calculated using the Antoine equation [41] which describes the relation between saturated temperature and saturated pressure of the vapor, as follows:

$$y_{int} = \frac{1}{P_{tot}} e^{(16.262 - \frac{3799.89}{T_{int} + 226.35})} \quad (2.12)$$

where the units of T_{int} and P_{tot} are *°C* and *kPa*, respectively. Based on the heat and mass transfer analogy (Lewis analogy) and equality of the Colburn j factors for heat and mass transfer [21], k_m is obtained from:

$$k_m = \frac{h_g M_{H_2O}}{c_{p,g} M_g y_{\ell m} Le_{H_2O-g}^{2/3}} \tag{2.13}$$

where $c_{p,g}$ is the specific heat of flue gas, and $Le_{H2O\text{-}g}$ is the Lewis number of water vapor in the flue gas. Moreover, y_{lm} is the logarithmic mole fraction difference of the non-condensable gas between the free stream and the wall [21] and is defined as:

$$y_{\ell m} = \frac{y_{ni} - y_{nb}}{Ln(y_{ni}/y_{nb})} \tag{2.14}$$

where y_{ni} and y_{nb} are the mole fraction of non-condensable gasses at the interface and in the bulk of flue gas [21].

In absence of condensation, solving the energy balance (Eq. (2.8)) results in finding the tube's outer surface temperature, denoted by $T_{w,o}$; thus, the amount of sensible heat transferred from flue gas flow to the HTF flow can be calculated using Eq. (2.15). The sensible heat transfer leads to a decrease in the flue gas temperature and an increase in the HTF temperature. In this case, the outlet temperature of the HTF and flue gas are calculated using Eq. (2.16) and (2.17).

$$Q_{non-cond} = h_g A_o (T_{g,bulk} - T_{w,o}) \tag{2.15}$$

$$T_{g,out} = T_{g,in} - \frac{Q_{non-cond}}{\dot{m}_g c_{p,g}} \tag{2.16}$$

$$T_{HTF,out} = T_{HTF,in} + \frac{Q_{non-cond}}{\dot{m}_{HTF} c_{p,HTF}} \tag{2.17}$$

where, $\dot{m}_g$ and $\dot{m}_{HTF}$ are the mass flow rate of the gas flow and the HTF flow, respectively. In the presence of condensation, the interface temperature is calculated by solving the energy balance (Eq. (2.9)). In this case, sensible heat transferred from the flue gas to the HTF leads to a decrease in the flue gas temperature. Moreover, the condensation rate

dictates the amount of latent heat transferred to the HTF flow. Also, the total heat, including both latent and sensible, transferred to the HTF flow causes an increase in the HTF temperature. Therefore, in the presence of condensation, the outlet temperature of HTF flow and flue gas along with the condensation rate are calculated using Eq. (2.18) - (2.20).

$$T_{g,out} = T_{g,in} - \frac{h_g A_o \, (T_{g,bulk} - T_{int})}{\dot{m}_g c_{p,g}} \tag{2.18}$$

$$T_{HTF,out} = T_{HTF,in} + \frac{(T_{int} - T_{HTF,bulk})}{\dot{m_{HTF}} c_{p,HTF} (R_{tube} + R_{HTF})} \tag{2.19}$$

$$\dot{m}_{cond} = \frac{\dot{Q}_{cond}}{h_{fg}} \tag{2.20}$$

A code was developed using MATLAB to solve the energy balance equation (Eq. (2.8) or (2.9)) using Newton-Raphson method [42] based on the above description, where 10^{-6} is considered as the convergence criterion. A typical crossflow tube-bank CHEX with in-line tube arrangement is schematically shown in Figure 2.4; the orange and blue arrows show the flue gas and HTF flow directions. Moreover, it schematically demonstrates how a tube-bank heat exchanger is modeled using the unit cell approach. The model considers the heat exchanger as a group of parallel tubes with identical diameter, spacing, and total length (Figure 2.4). The length of U-shaped parts of a tube should be added to the length of the straight part of it if they contribute to heat transfer. Since the tube surface of unit cells are assumed isothermal, the number of unit cells along the tubes should be chosen in a way that having more unit cells along the tubes does not affect the results.

It should be noted that the unit cells have the same geometry but different inlet conditions. The model solves the energy balance for unit cells along the liquid flow direction, from inlet to outlet. For each unit cell, the steps that the model takes can be summarized as follows:

- Take the inlet humidity ratio, temperature, and mass flow rate of the gas and the inlet temperature and mass flow rate of the HTF flow as the model's input parameters

- Solve the energy balance on the tube's surface (Eq. (2.8) or (2.9)) based on the thermal resistance networks (Figure 2.3) to find the interface temperature and the mole fraction of water vapor at the interface

- Calculate the condensation rate and the outlet temperatures of the HTF and gas for the unit cell (the model's output) using Eq. (2.15) - (2.20).

- Update the inputs of the next unit cell based on the outputs of the adjacent unit cells (based on flow directions of the gas flow and the HTF flow)

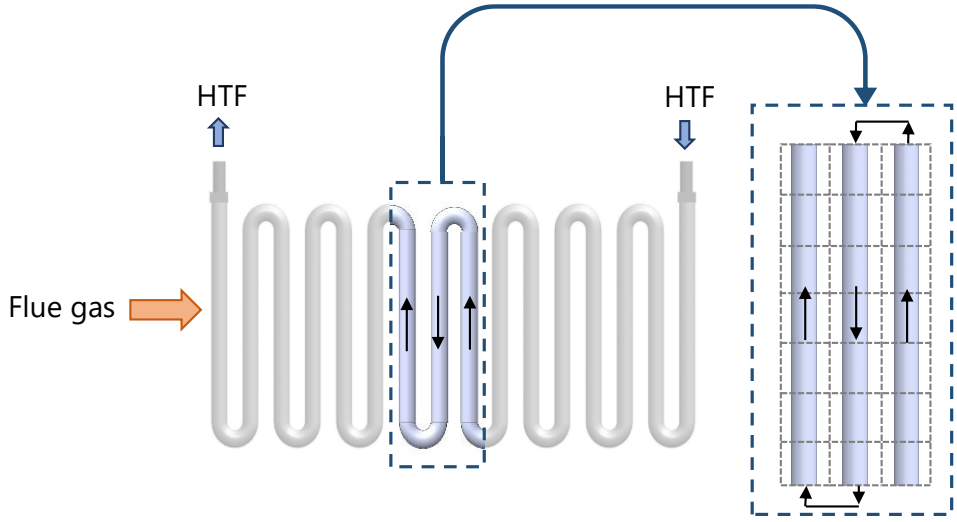

Figure 2.4. A typical tube-bank heat exchanger with in-line tube arrangement; the dashed box shows the geometry considered by the model to solve heat and mass transfer of the highlighted portion of the tube bundle.

As shown in Figure 2.5, the flue gas inlet conditions of unit cells are specified based on the outlet conditions of their adjacent cells in the upstream gas direction. Moreover, for unit cells along the tubes, a typical one highlighted in red color, the inlet HTF temperature is considered equal to the outlet HTF temperature of its adjacent cell in the upstream HTF flow direction. However, for unit cells placed at the top and bottom end of the tubes, a typical one highlighted in red color, the inlet HTF temperature is considered equal to the outlet HTF temperature of the previous tube along the HTF flow direction.

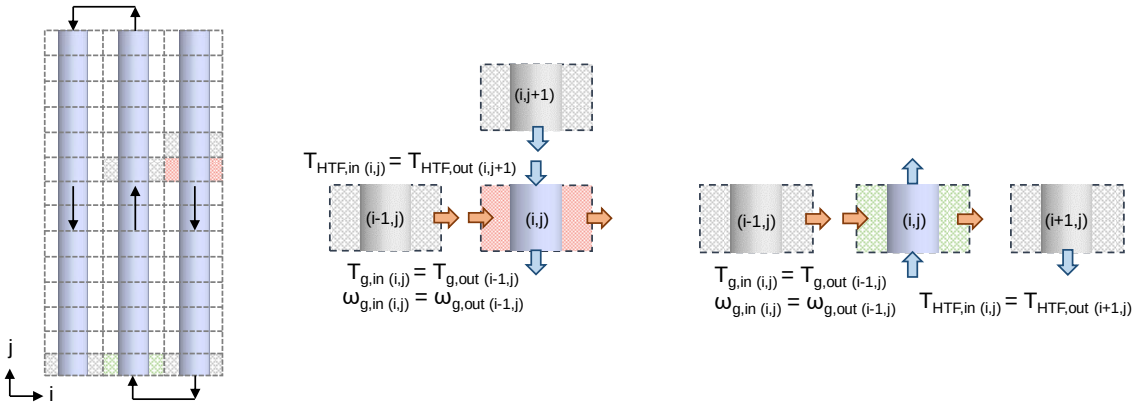

Figure 2.5. The inlet conditions of unit cells; red highlighted unit cell is a typical unit cell along the tubes, and green-highlighted unit cell is a typical unit cell placed at the end of tubes; the adjacent cells which affect the inlet condition of these unit cells are highlighted by grey color.

2.2. Preliminary Model validation

The present model was verified using the experimental data reported by Jeong et al. [21]. They tested five heat exchangers connected in series and placed inside a duct through which the flue gas was flowing. All the details regarding the dimensions of heat exchangers can be found in Ref. [21]. The temperature profiles of flue gas and HTF along the heat exchangers and the condensation rate of each heat exchanger were reported for an experimental test in which the inlet temperature of the HTF and the flue gas were 31°C and 149.5°C, respectively, and the inlet moisture fraction of flue gas was 14.4 vol%. Moreover, the mass flow rate of HTF and flue gas were 542.9 $kg \cdot h^{-1}$ and 185.7 $kg \cdot h^{-1}$, respectively. The modeling results for temperature profiles of the flue gas and HTF along the five heat exchangers were compared with the experimental data reported by Jeong et al. [21] (Figure 2.6). It should be mentioned that the flue gas entered the heat recovery system through the first heat exchanger, while the HTF entered the system through the fifth one. The flue gas and HTF flow directions are shown schematically in Figure 2.7. Moreover, condensation rates of individual heat exchangers along with the total amount of condensation were compared with experimental data reported by Ref. [21]. Maximum discrepancy between the experimental data and the modeling results for condensation rates of individual heat exchangers was within 15% and for the total condensation rate of heat exchangers was within 5%.

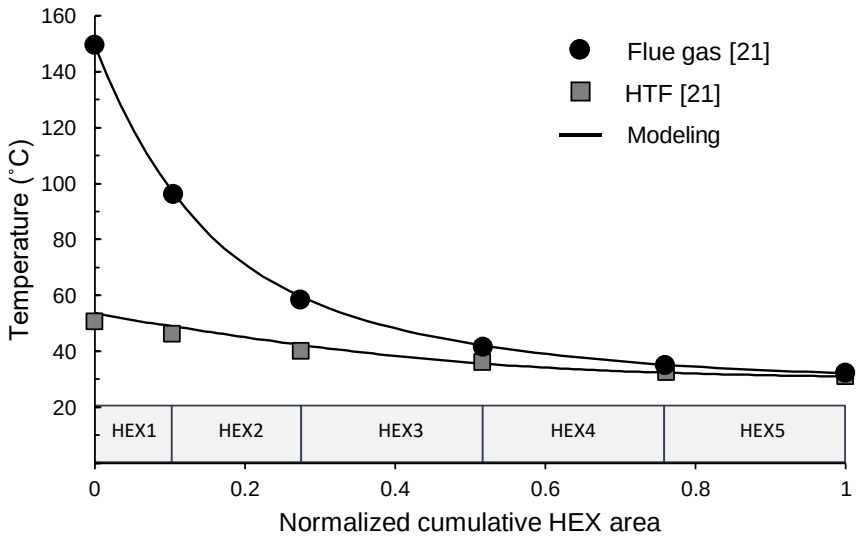

Figure 2.6. Comparison between predicted and measured temperature profiles of flue gas and HTF along the heat exchangers; experimental data reported by Jeong et al. [21]**.**

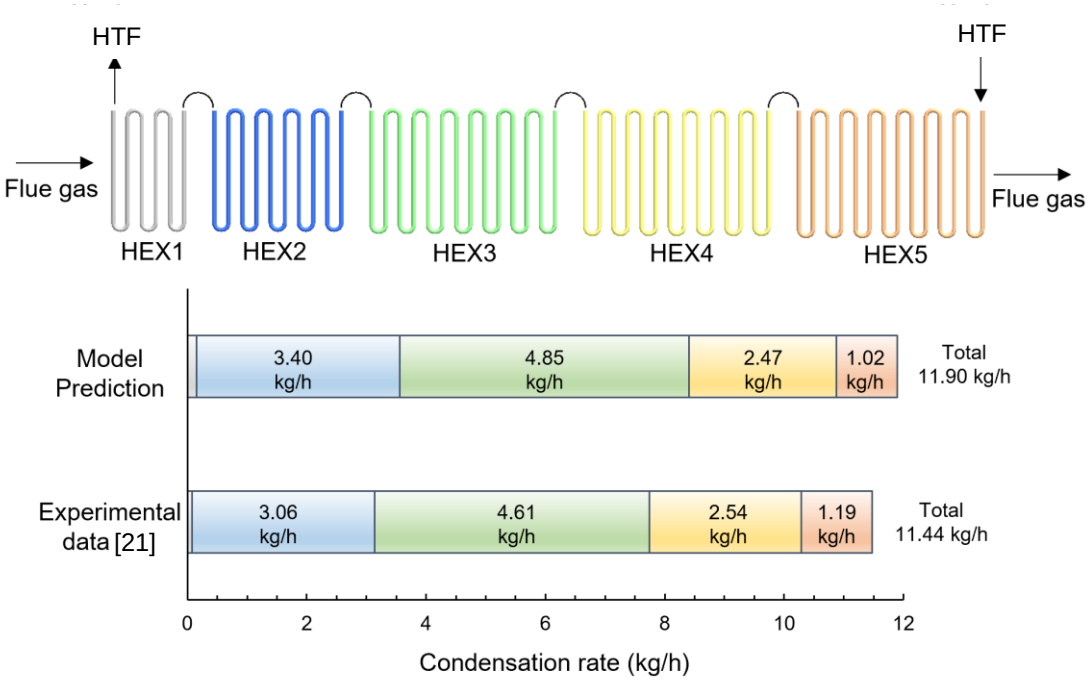

Figure 2.7. Comparison between the model predictions and experimental data of total and individual condensation rates of five heat exchangers; experimental data reported by Jeong et al. [21]**.**

Chapter 3.

Performance evaluation of CHEXs made of different materials

To further evaluate the performance of CHEXs made of different materials, a lab-scale experimental testbed was designed to investigate the significance of material's thermal conductivity. Moreover, the analytical model developed in this thesis was validated for two different extremes of thermal conductivity using the experimental results of this chapter.

3.1. Thermal and hydraulic performance of HWRUs

The performance of a CHEX is investigated using key performance indicators defined in Table 3.1:

Table 3.1. Key performance indicators for a CHEX

Parameter	Definition
Water recovery efficiency (-)	$\boldsymbol{WRE = \frac{\dot{m}_{cond}}{\dot{m}_{v,in}}}$
Heat recovery efficiency (-)	$\boldsymbol{HRE = \frac{\dot{m}_{cond}h_{fg} + \dot{m}_g c_{p,g}(T_{g,in} - T_{g,out})}{\dot{m}_{v,in}h_{fg} + \dot{m}_g c_{p,g}(T_{g,in} - T_{HTF,in})}}$
Total heat recovery rate ($\boldsymbol{W}$)	$\boldsymbol{HR = \dot{m}_{HTF} c_{p,HTF}(T_{HTF,out} - T_{HTF,in})}$
Flue gas pressure drop ($\boldsymbol{Pa}$)	$\boldsymbol{\Delta P_g}$
HTF pressure drop ($\boldsymbol{Pa}$)	$\boldsymbol{\Delta P_{HTF}}$

The water recovery efficiency is defined as the condensation rate over the mass flow rate of water vapor in the flue gas at the inlet of a CHEX. In other words, this parameter shows what percentage of water vapor can be recovered from flue gas using the CHEX. Water recovery efficiency also shows the performance of the system in

recovering latent heat of flue gas. Moreover, the heat recovery efficiency of an HWRU is defined as the ratio of the total heat recovery rate over the maximum possible heat recovery rate. The change in specific heat of the flue gas as a result of the condensation can is less that 3 percent and can be neglected. Heat recovery efficiency assesses both sensible and latent heat recovery of the unit. It should be noted that it is not desirable to cool down the flue gas to reach the inlet temperature of HTF flow and recover as it affects the flue gas discharge at the stack. Since the share of the sensible heat is negligible compared to the share of the latent heat, the value of heat recovery efficiency is close to the value of water recovery efficiency (Appendix A). Therefore, the water recovery efficiency and the total heat recovery are considered as the CHEX thermal performance indicators.

The total heat recovery rate is calculated based on the temperature increase of the HTF as a result of both sensible and latent heat, recovered from the wet exhaust stream. Furthermore, like any other HEXs, the pressure drops of both the flue gas flow and the HTF flow should be considered to fully assess the performance of a CHEX.

3.2. Experimental testbed

A custom-built CHEX with replaceable tubes was designed and built in Laboratory for Alternative Energy Conversion (LAEC) to validate the analytical model for different tube materials and a range of working conditions (see Figure 3.1). The main geometrical parameters of the unit are listed in Table 3.2. To make the tubes replaceable, push-in u-bends (John Guest, UK) were used to connect the tubes, as shown in Figure 3-2. The bends were placed outside of the frame and were insulated to make sure that there was no heat loss to ambient through them.

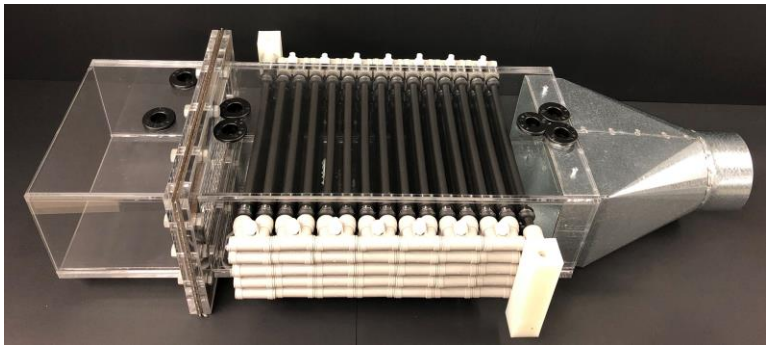

Figure 3.1. Custom-built CHEX with replaceable tubes.

Table 3.2. Summary of geometrical parameters of the custom-built CHEX

Outer tube diameter	9.5 mm
Tube thickness	0.8 mm
Tube length, placed inside the frame	210 mm
Number of tubes – transversal direction	5
Number of tubes – longitudinal direction	15
Tube pitch – transversal direction	21.7 mm
Tube pitch – longitudinal direction	21 mm

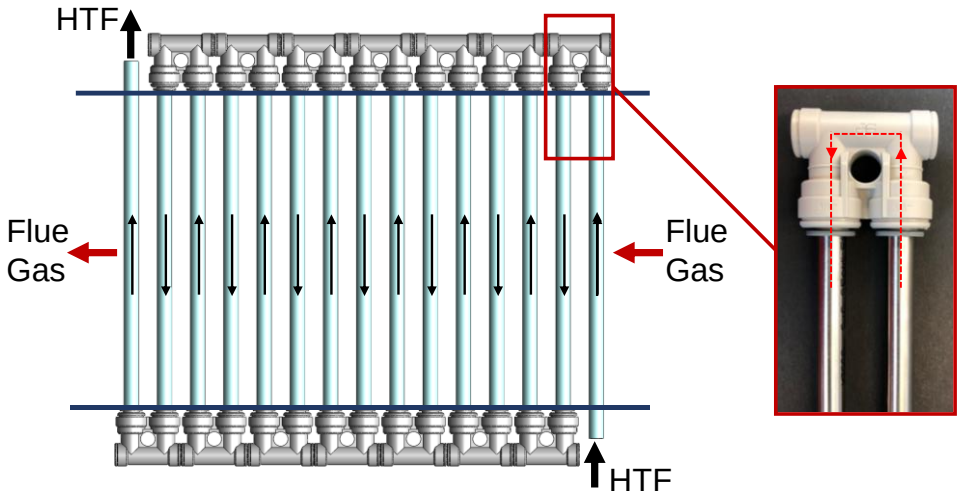

Figure 3-2. Schematic showing the flow of the HTF and flue gas through the CHEX, where the tubes are connected using reusable push-in u-bends.

As shown in Figure 3-3, the headers distribute the HTF flow equally among five parallel paths and mix them at the outlet. The main advantage of having the custom-designed CHEX was the feasibility of changing the tubes while keeping all other geometrical parameters identical. Moreover, a P-trap was installed on the bottom of the testbed to collect the recovered water and prevent air from entering the unit while allowing the recovered water to pass through the discharge hole on the bottom of the CHEX.

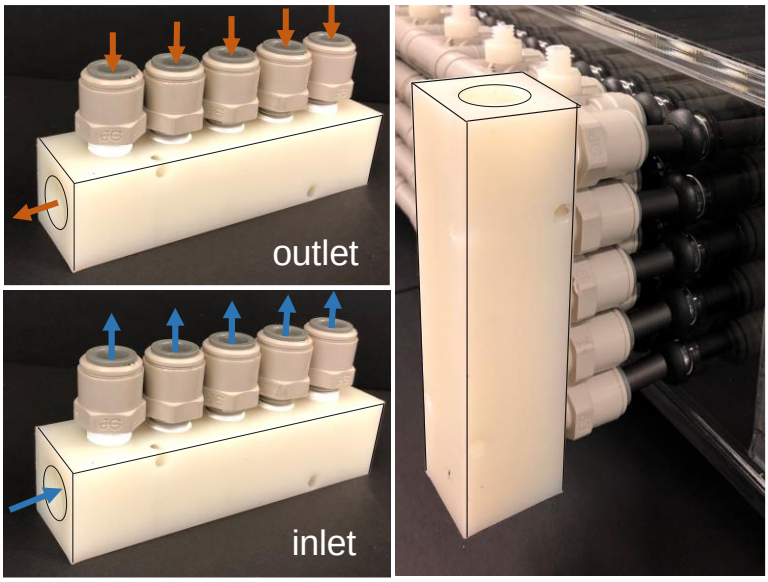

Figure 3-3. Headers located at the inlet and outlet of the CHEX.

A testbed, schematically shown in Figure 3.4, was designed and built to measure the thermal and hydraulic performance of the CHEX. A temperature control system (FL4003, Julabo) was used to circulate the HTF through the CHEX tubes and keep the inlet temperature constant. The inlet and outlet HTF temperatures were measured using two RTD sensors (Pt100, OMEGA) installed before and after the HWRU. The HTF flow rate was measured using an oval gear flow meter (OM015S001, FLOMEC) and controlled using a valve. Further, two pressure transmitters (PX305-100 GI, OMEGA) were installed before and after the unit to measure the pressure drop of the HTF flow.

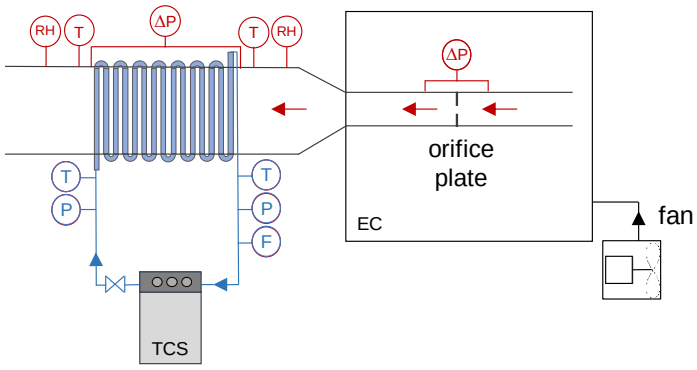

Figure 3.4. Schematic of the experimental test bed; blue arrows: HTF flow; red arrows: flue gas flow; EC: environmental chamber; TCS: temperature control system; T: temperature sensor; P: pressure sensor; RH: relative humidity sensor; F: liquid flow meter.

To mimic the flue gas conditions in the lab, the inlet temperature and humidity ratio of the gas were set using a standard environmental chamber (SE-3000-10-10, Thermotron). The chamber is capable of setting the temperature and relative humidity within -70 to +180°C and 10-98%RH, respectively. The gas flow rate was controlled using a variable-speed axial fan. The flow rate of the gas was measured using an orifice plate (Oripac 4150T, Lambdasquare) mounted inside a circular duct using standard flanges. The orifice plate and the circular ducts connected to both sides of the orifice plate were placed inside of the environmental chamber to avoid condensation inside of the circular ducts. The pressure-drop of the gas passing through the orifice plate was measured using a differential pressure sensor (2671005WB2DA1FD, Setra). Moreover, RTD sensors (Pt100, OMEGA) and relative humidity sensors (HMP110, Vaisala) were installed before and after the CHEX to measure the inlet and outlet temperature and humidity ratio of the gas. Moreover, the gas pressure drop was measured using a differential pressure sensor (2671R25WB2DA1FN, Setra). The mass of recovered water was measured using a scale (ML4002E, Mettler Toledo). The testbed was insulated to minimize the heat loss to ambient and make sure that the entire recovered sensible and latent heat of gas was transferred to the HTF flow. More details related to the sensors including their ranges and uncertainties are listed in Table 3.3.

Table 3.3. Summary of sensors utilized in the testbed for data measurment

Sensor	Model	Range	Uncertainty
Temperature sensor	RTD (Pt100) - OMEGA	-200 to 500°C	0.15°C
Flow meter	OM015S001- FLOMEC	0 to 40 lit.min^{-1}	0.5%
Pressure transmitter	PX305 - OMEGA	0 to 100 psi	0.25% FS
Differential pressure sensor	2671005WB2DA1FD - Setra	± 5″ W.C	0.25% FS
	2671R25WB2DA1FN - Setra	± 0.25″ W.C	0.25% FS
Humidity sensor	HMP110 - Vaisala	0 to 100%	3%RH (at 40-80°C)
Scale	ML4002E, Mettler Toledo	0 to 5000 g	0.01 g

The mass flow rate of the gas was calculated based on the pressure drop measurements through the orifice plate, as per ISO standard 5167 [43], as:

$$\dot{m}_{g,in} = \frac{C'}{\sqrt{1-\beta^4}} \varepsilon \frac{\pi}{4} d^2 \sqrt{2\Delta P \rho_{g,in}} \tag{3.1}$$

where *C'* is coefficient of discharge, *β* is diameter ratio, *ε* is expansion factor, and *d* is the orifice diameter. The coefficient of discharge can be found from [43]:

$$C = 0.5961 + 0.0261\beta^2 - 0.216\beta^8 + 0.000521(10^6\,\beta/Re_D)^{0.7} + (0.0188 + 0.0063A)\beta^{3.5}(10^6/Re_D)^{0.3} - 0.031\left(\acute{M}_2 - 0.8\acute{M}_2^{\,1.1}\right)\beta^{1.3} + (0.043 + 0.080e^{-10L_1} - 0.123e^{-7L_1})(1 - 0.11A)\,(\beta^4/1-\beta^4) \tag{3.2}$$

where Re_D is the Reynolds number of the gas flow with respect to the diameter (*D*) of the pipes, connected to the orifice plate. The other parameters are defined as follows [43]:

$$\beta = d/D \tag{3.3}$$

$$A = (19000\beta/Re_D)^{0.8} \tag{3.4}$$

$$\acute{M}_2 = 2L_2/(1-\beta) \tag{3.5}$$

$$L_2 = L_1 = 0.0254/D \tag{3.6}$$

The expansion factor is also defined as [43]:

$$\varepsilon = 1 - (0.351 + 0.256\beta^4 + 0.93\beta^8)\left[1 - (p_2/p_1)^{1/\kappa}\right] \tag{3.7}$$

where, *κ* is the isentropic exponent. The orifice diameter of Oripac 4150T with diameter ratio of 2 was 2 inches.

3.3. Uncertainty analysis

Due to the uncertainties of sensors and standard deviation of readings, there are uncertainties in the measured performance parameters that should be calculated based on the standard method developed by Moffat [44].

The total heat recovery rate (*HR*) is calculated from measurements of RTD temperature sensors and the liquid flow meter. The uncertainty of this parameter is calculated as:

$$\left(\frac{\delta HR}{HR}\right)^2 = \left(\frac{\delta \rho}{\rho}\right)^2 + \left(\frac{\delta \dot{V}_{HTF}}{\dot{V}_{HTF}}\right)^2 + \left(\frac{\delta c_{p,HTF}}{c_{p,HTF}}\right)^2 + \left(\frac{\delta\left(T_{HTF,out} - T_{HTF,in}\right)}{\left(T_{HTF,out} - T_{HTF,in}\right)}\right)^2, \tag{3.8}$$

$$\delta\left(T_{HTF,out} - T_{HTF,in}\right)^2 = \delta\left(T_{HTF,out}\right)^2 + \delta\left(T_{HTF,in}\right)^2 \tag{3.9}$$

where, $\dot{V}_{HTF}$ is the volume flow rate of the HTF. It should be mentioned that the uncertainties of thermodynamics properties of the HTF including its density and specific heat are neglected. Therefore, the uncertainty of the total heat recovery rate (*HR*) is written as:

$$\frac{\delta HR}{HR} = \left[\left(\frac{\delta \dot{V}_{HTF}}{\dot{V}_{HTF}}\right)^2 + \frac{\delta\left(T_{HTF,out}\right)^2 + \delta\left(T_{HTF,in}\right)^2}{\left(T_{HTF,out} - T_{HTF,in}\right)^2}\right]^{1/2}. \tag{3.10}$$

Considering the uncertainties of sensors listed in Table 3.3 and the values of parameters, the maximum uncertainty of total heat recovery rate measurements was 9%. The uncertainties of the water recovery efficiency (*WRE*) and heat recovery efficiency (HRE) are calculated as:

$$\left(\frac{\delta WRE}{WRE}\right)^2 = \left(\frac{\delta \omega}{1+\omega}\right)^2 + \left(\frac{\delta \omega}{\omega}\right)^2 + \left(\frac{\delta \dot{m}_{cond}}{\dot{m}_{cond}}\right)^2 + \left(\frac{\delta \dot{m}_{g,in}}{\dot{m}_{g,in}}\right)^2 \text{ and} \tag{3.11}$$

$$\left(\frac{\delta HRE}{HRE}\right)^2 = \left(\frac{\delta HR}{HR}\right)^2 + \left(\frac{\delta Q_{max}}{QQ_{max}}\right)^2 \tag{3.12}$$

where, Q_{max} is the maximum possible heat recovery rate and is defined as follows:

$$Q_{max} = \dot{m}_{g,in}\frac{\omega}{1+\omega}h_{fg} + \dot{m}_{g,in}c_{p,HTF}\left(T_{g,in} - T_{HTF,in}\right) \tag{3.13}$$

$$(\delta Q_{max})^2 = \left(\dot{m}_{g,in}\frac{\omega}{1+\omega}h_{fg}\right)^2\left[\left(\frac{\delta\dot{m}_{g,in}}{\dot{m}_{g,in}}\right)^2 + \left(\frac{\delta\omega}{1+\omega}\right)^2 + \left(\frac{\delta\omega}{\omega}\right)^2\right] + \tag{3.14}$$

$$\left(\dot{m}_{g,in}c_{p,HTF}\left(T_{g,in}-T_{HTF,in}\right)\right)^2\left[\left(\frac{\delta\dot{m}_{g,in}}{\dot{m}_{g,in}}\right)^2 + \frac{\delta\left(T_{g,in}\right)^2 + \delta\left(T_{HTF,in}\right)^2}{\left(T_{g,in}-T_{HTF,in}\right)^2}\right]$$

To calculate the uncertainty of these parameters, the uncertainty of the gas humidity ratio (ω) at the inlet of the unit should be calculated based on the uncertainty of readings of humidity and temperature sensors located before the CHEX. Considering the uncertainties of sensors listed in Table 3.3 and the values of parameters, the maximum uncertainty of water recovery efficiency was 3.5% for the range of inlet conditions tested in this study.

Inlet humidity ratio (ω) of the gas is defined as:

$$\omega_{in} = 0.622\,P_{sat}RH_{in}/(P_{tot} - P_{sat}RH_{in}), \tag{3.15}$$

where P_{sat} is the saturation pressure of the vapor at the inlet temperature and can be calculated as:

$$P_{sat} = e^{\left(16.262-\frac{3799.89}{T_{g,in}+226.35}\right)} \tag{3.16}$$

where the units of $T_{g,in}$ and P_{sat} are °C and kPa, respectively. Based on the law of propagation of uncertainty, the uncertainty of the inlet gas humidity ratio of is calculated as:

$$(\delta\omega_{in})^2 = (d\omega_{in}/dP_{sat})(\delta P_{sat})^2 + (d\omega_{in}/dRH_{in})(\delta RH_{in})^2 + (d\omega_{in}/dP_{tot})(\delta P_{tot})^2 \tag{3.17}$$

where

$$d\omega_{in}/dP_{sat} = 0.622P_{tot}RH_{in}/(P_{tot} - P_{sat}RH_{in})^2, \tag{3.18}$$

$$d\omega_{in}/dRH_{in} = 0.622P_{tot}P_{sat}/(P_{tot} - P_{sat}RH_{in})^2, \tag{3.19}$$

$$d\omega_{in}/dP_{tot} = 0.622\, P_{sat} RH_{in}/(P_{tot} - P_{sat} RH_{in})^2, \text{and} \tag{3.20}$$

$$\delta P_{sat} = \left[\left(1000 * 3799.89/\left(T_{g,in} + 226.35\right)^2\right) \times e^{\left(16.262 - \frac{3799.89}{T_{g,in}+226.35}\right)}\right]^{1/2} (\delta T_{g,in}). \tag{3.21}$$

More details about the derivation of uncertainties for different parameters can be found in Appendix B. The uncertainty of the mass flow rate of gas, as per ISO standard 5167, can be obtained from the following equation [43]:

$$\frac{\delta \dot{m}_{g,in}}{\dot{m}_{g,in}} = \left[\left(\frac{\delta C}{C}\right)^2 + \left(\frac{\delta \varepsilon}{\varepsilon}\right)^2 + \left(\frac{2\beta^4}{1-\beta^4}\right)^2 \left(\frac{\delta D}{D}\right)^2 + \left(\frac{2}{1-\beta^4}\right)^2 \left(\frac{\delta d}{d}\right)^2 + \frac{1}{4}\left(\frac{\delta \Delta p}{\Delta p}\right)^2 + \frac{1}{4}\left(\frac{\delta \Delta \rho_1}{\Delta \rho_1}\right)^2\right]^{1/2}. \tag{3.22}$$

3.4. Assessment of the test bed insulation

In order to prevent any heat loss to the ambient, the testbed was insulated using extruded polystyrene rigid insulation covered by a layer of foam insulation (see Figure 3-5 a). As shown in Figure 3-5 b, the image taken from the testbed during the tests using a portable IR camera (i7, FLIR) showed that the surface temperature of the testbed was close to the ambient temperature during the tests in spite of the significant temperature difference between the gas flow and ambient.

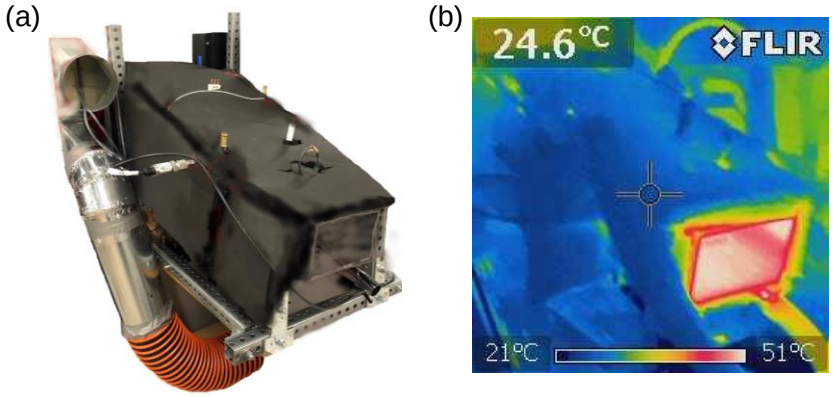

Figure 3-5. (a) The experimental test bed after insulation; (b) an IR image of the testbed during the tests.

In the case of perfect insulation, heat transfer occurs only between the HTF and the gas flow. In other words, the recovered sensible and latent heat from the gas flow is transferred to the HTF flow, increasing the temperature of the HTF flow. To assess the insulation of

the test bed, the balance between the amount of heat gained by the HTF flow and the amount of heat transferred from the gas flow was investigated to make sure that there was no heat loss from the testbed to the ambient. For some of the tests conducted in this study, Figure 3.6 shows the heat transfer rate of the HTF flow in comparison with the sensible and latent heat recovery rates from the gas flow, for a range of HTF volumetric flow rates. The inlet conditions of these tests are listed in Table 3.4. Moreover, the heat balance was tested for a range of different inlet conditions, see Figure 3-7. As shown in Figure 3.6 and Figure 3-7, there is a proper balance (within the error range) between the amount of heat transferred to the HTF flow and the total heat, including both sensible and latent heat, transferred from the gas flow, which indicates the proper insulation of the test bed.

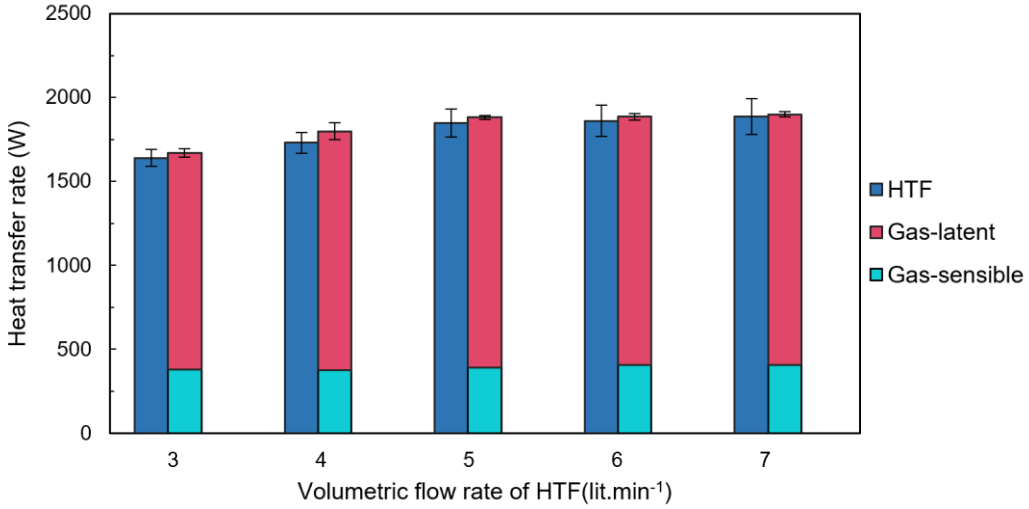

Figure 3.6. Heat transfer rates of the gas flow and the HTF flow.

Table 3.4. Summary of the test conditions for the data of Figure 3.6

Tube material	FEP plastic
Inlet HTF temperature	25.0°C
Inlet gas temperature	70°C
Mass flow rate of the gas	80 $kg \cdot h^{-1}$
Volumetric flow rate of HTF	3-7 $lit.min^{-1}$
Inlet gas humidity ratio	100 $g_{H2O}/kg_{dry\text{-}air}$

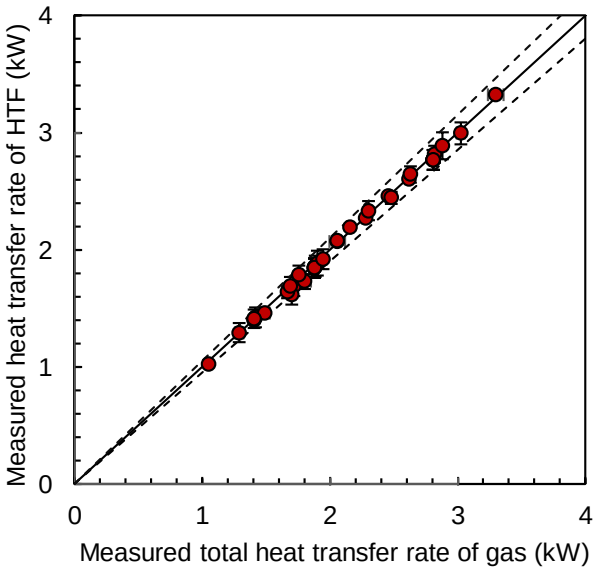

Figure 3-7. Measured heat transfer rate of HTF vs. total heat transfer rate of gas for all the tests.

3.5. Parametric study on the performance of CHEXs

A comprehensive parametric study was performed for two CHEXs made of 304 stainless-steel tubes and plastic FEP tubes to validate the model for relatively low and high ranges of thermal conductivity of tube materials and different inlet conditions. A set of inlet conditions was considered as the baseline case, listed in Table 3.5. Then, each parameter was varied over a chosen range while all the other inlet conditions were kept constant to investigate the effects of each parameter on the performance metrics of the CHEX, including total heat recovery rate and water recovery efficiency. Further, the effects of each parameter on pressure drop in the flue gas and HTF were studied experimentally.

Figure 3-8 a shows heat and mass transfer resistance networks for condensation of flue gas in an HWRU. In the mass resistance network, R_m is the mass transfer resistance linking the concentration of water vapor in the bulk of the flue gas ($C_{g,bulk}$) to the concentration of water vapor on the interface between the flue gas and the condensate layer (C_{int}). As a result of condensation, the latent heat of condensation (Q_{cond}) is released on the interface between the condensate layer and the flue gas. Figure 3-8 b shows a simplified thermal resistance network where R_{fg} is the equivalent thermal resistance for the total heat transfer between the flue gas and the outer surface of the tube.

Table 3.5. Inlet conditions of the baseline case defined for the parametric study and the model validation.

Inlet HTF temperature	25.0°C
Inlet gas temperature	70°C
Mass flow rate of the gas	80 $kg \cdot h^{-1}$
Volumetric flow rate of the HTF	5 $lit.min^{-1}$
Inlet gas humidity ratio	100 $g_{H2O}/kg_{dry\text{-}air}$

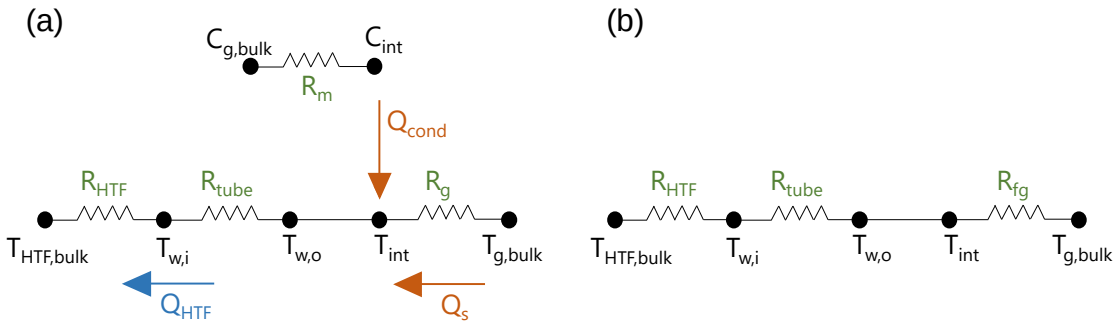

Figure 3-8. (a) Thermal and mass resistance networks and (b) equivalent thermal resistance network of flue gas condensation on a tube surface;

Figure 3-9 shows the variation of performance indicators and thermal resistances with increasing the mass flow rate of the flue gas for both the stainless-steel condensing heat exchanger (SCHEX) and the plastic condensing heat exchanger (PCHEX). Increasing the mass flow rate of the flue gas leads to an increase in the Nusselt number and, consequently, a higher convective heat transfer coefficient for the gas. Therefore, based on Lewis analogy, the mass transfer coefficient of the gas increases and results in a higher condensation rate and, consequently, a higher latent heat recovery rate (see Eq. (2.13)). Moreover, the sensible heat recovery rate from the gas flow increases due to the lower convective resistance between the gas flow and the tube wall (see Eq. (2.2)). As a result, R_{fg} decreases by increasing the flow rate of the flue gas, as shown in Figure 3-9 c. Therefore, increasing the mass flow rate of the flue gas results in a significant increase in the total heat recovery rate (see Figure 3-9 a). However, as shown in Figure 3-9 a, the rate of increase for the SCHEX is significantly higher than the PCHEX. The reason behind

these trends is the effect of the interface temperature (T_{int}). The interface temperature of the SCHEX is much lower than PCHEX due to smaller resistance of tube wall (shown in Figure 3-9 c), which leads to a lower mole fraction of the water vapor on SCHEX's interface and a larger difference between the mole fraction of the vapor in the bulk of the gas and the vapor on the interface. Moreover, increasing the mass flow rate of flue gas results in the higher bulk temperature of flue gas and therefore higher interface temperature. Therefore, there is a trade-off between the higher interface temperature and the higher convective heat and mass transfer rate of the gas. Xiong et al. [14] observed a significant reduction in the heat recovery rate of the plastic heat exchanger with increasing the flue gas velocity within the range of inlet conditions that they considered. All these results show that there is an optimum flue gas flow rate (velocity) to reach the maximum heat recovery rate for a specific set of inlet conditions.

As shown in Figure 3-9 b, by increasing the mass flow rate of the flue gas, the mass flow rate of the water vapor entering the CHEX increases. Although increasing the mass flow rate of the flue gas leads to enhancement in the condensation rate, it eventually leads to deterioration of the water recovery efficiency. The reason for this observation is that the augmentation in the mass flow rate of the entering water vapor (in the denominator of the efficiency) is more than the enhancement in the condensation rate (in the numerator of the efficiency). In other words, within the range of inlet conditions considered for the parametric study, the water recovery efficiency of the unit, with a specific size, drops when the mass flow rate of the gas increases although it enhances the total heat recovery of the unit.

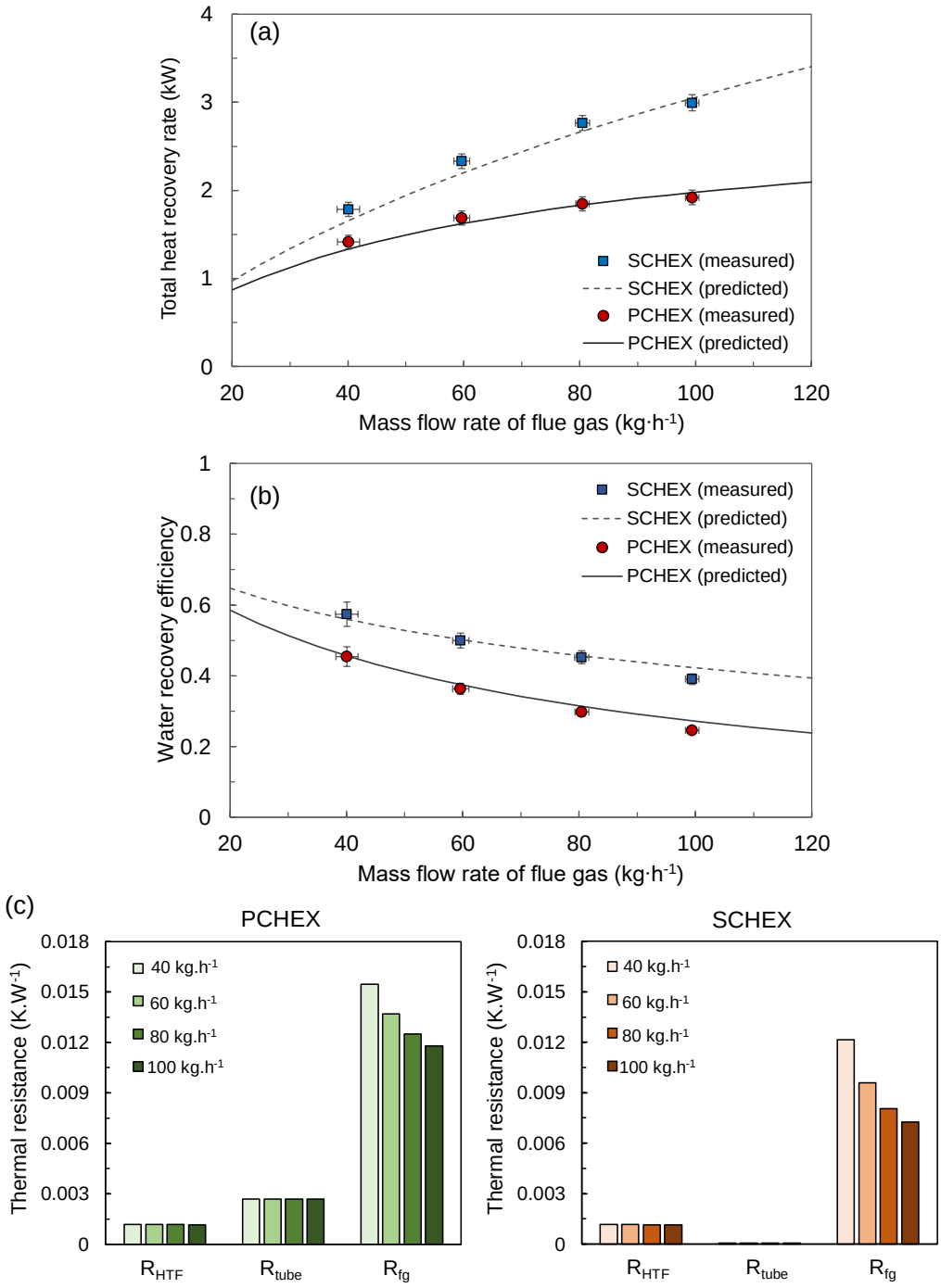

Figure 3-9. Parametric study: variation of (a) total heat recovery rate, (b) water recovery efficiency, and (c) thermal resistances of the network, shown in Figure 3-8 b, with inlet mass flow rate of flue gas.

Figure 3-10 represents the effect of flue gas humidity ratio on the total heat recovery rate and the water recovery efficiency of SCHEX and PCHEX. It is worth mentioning that the humidity ratio of the flue gas depends on the type of fuel burning in

the boiler. For example, the humidity ratio of 100 $g_{H2O}/kg_{dry\text{-}air}$ approximately corresponds to the flue gas of boilers burning natural gas. Higher humidity ratio of the flue gas corresponds to higher mole fraction of water vapor in the bulk of the gas. This leads to a bigger difference between the mole fraction of water vapor in the bulk of the gas and the interface between the gas and the condensate layer. As a result, for both SCHEX and PCHEX, R_{fg} decreases by increasing the humidity ratio of the flue gas, as shown in Figure 3-10. Therefore, as shown in Figure 3-10 a, the condensation rate and the latent heat recovery rate increases with increasing the inlet humidity ratio of the gas. However, in this case, despite the previous case, the enhancement in the condensation rate (in the numerator of the efficiency) is more than the augmentation in the mass flow rate of the entering water vapor (in the denominator of the efficiency). For this reason, the water recovery efficiencies of both CHEXs enhance by increasing the gas humidity ratio (see Figure 3-10 b). Moreover, higher values of R_{tube} for PCHEX result in higher interface temperature and higher values of R_{fg} compared to SCHEX.

Figure 3-11 shows the effect of HTF volumetric flow rate on heat and water recovery efficiency of the heat exchanger as well as the thermal resistances. Increasing the volumetric flow rate of the HTF flow leads to a decrease in the convective heat transfer resistance between the HTF flow and the internal walls of the tubes, as shown in Figure 3-11 c. As shown in Figure 3-11 a, this slightly increases the total heat recovery of the SCHEX but has a negligible effect on the total heat recovery rate of the PCHEX. The reason behind this observation could be the higher conductive resistance of the plastic tubes than the convective heat transfer resistance between the HTF and the internal walls of the tubes in the case of the PCHEX, see Figure 3-11 c. This also leads to an insignificant change in the interface temperature of the PCHEX as the convective resistance of the HTF decreases. Since in this case, the mass flow rate of the water vapor entering the heat exchanger (in the denominator of the efficiency) does not change, the same increasing trends are observed for the water recovery efficiency of the CHEXs (see Figure 3-11 b).

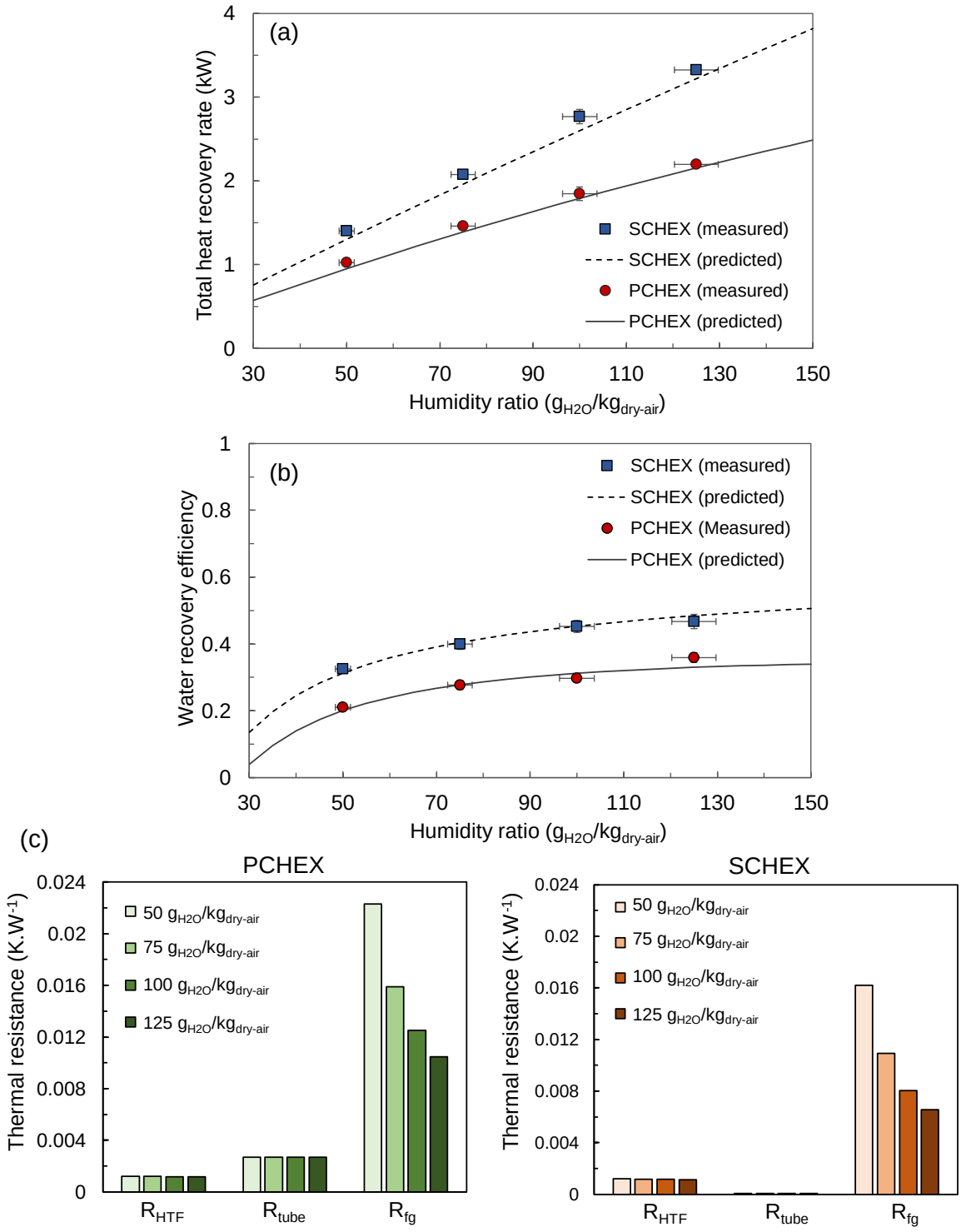

Figure 3-10. Parametric study: variation of (a) total heat recovery rate, (b) water recovery efficiency, and (c) thermal resistances of the network, shown in Figure 3-8 b, with inlet humidity ratio of the flue gas.

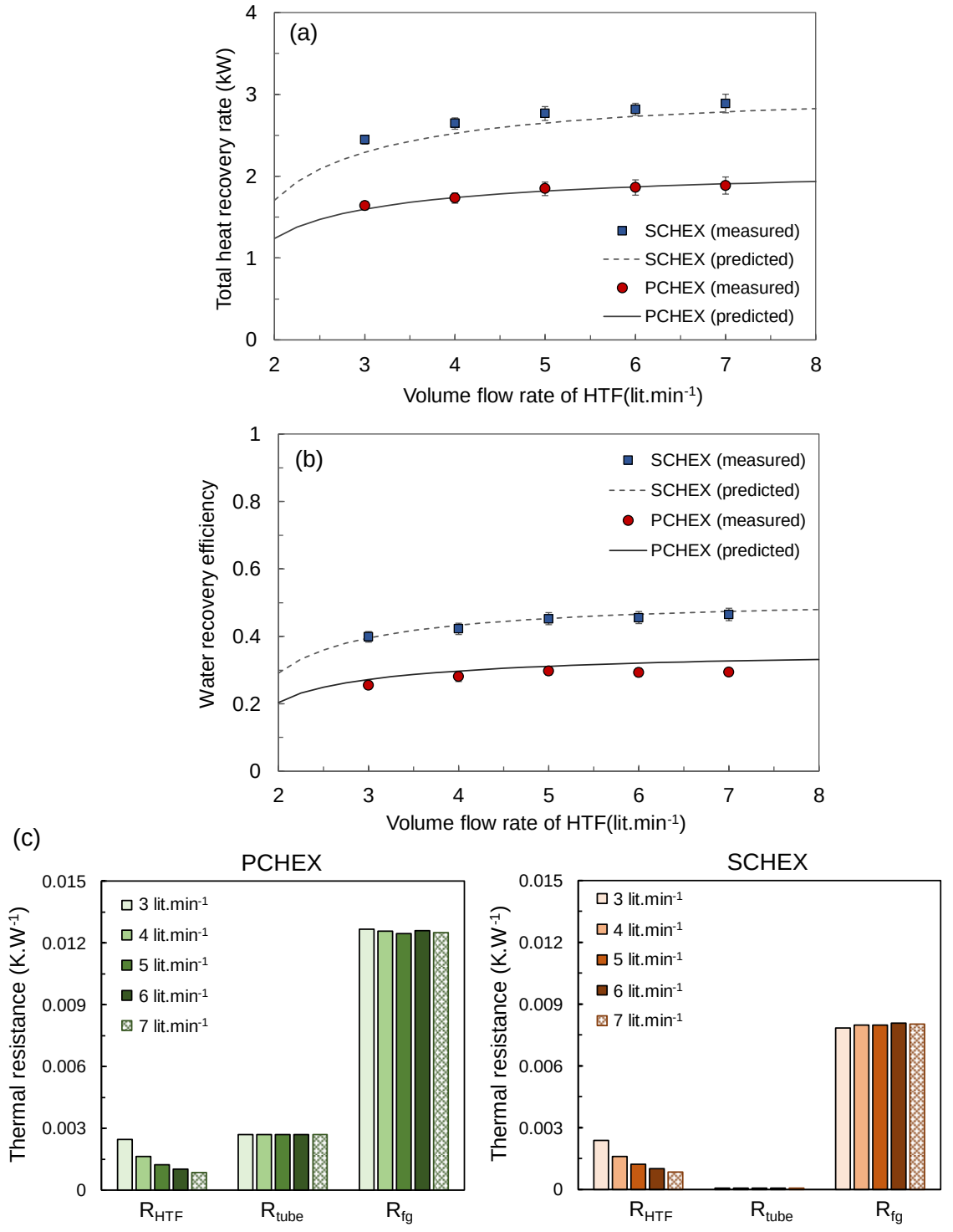

Figure 3-11. Parametric study: variation of (a) total heat recovery rate, (b) water recovery efficiency, and (c) thermal resistances of the network, shown in Figure 3-8 b, with inlet volume flow rate of HTF.

Figure 3-12 shows the variation of total heat recovery rate and water recovery efficiency of the CHEXs with the inlet temperature of the HTF. Increasing the inlet temperature of the HTF increases the interface temperature and, consequently, decreases the condensation rate and the total heat recovery rate. As shown in Figure 3-12 a and b, increasing the inlet temperature of the HTF has a more significant effect on the performance of the both CHEXs compared to increasing the flow rate of the HTF (see Figure 3-11 a and b). Although increasing the inlet temperature of the HTF doesn't change the R_{fg} significantly, as shown in Figure 3-12 c, it significantly affects the heat recovery rate and condensation efficiency (see Figure 3-12 a and b). The main reason for this observation is that increasing the HTF inlet temperature increases the bulk temperature of the HTF, which results in a lower temperature difference and lower heat and water recovery rates.

In addition to showing the effect of inlet conditions on the heat and water recovery performance of the SCHEX and PCHEX, Figure 3-10 to Figure 3-12 show the accuracy of the model in predicting the performance of a CHEX. As can be seen in these figures, the model successfully captures the trends of the data within the chosen range of inlet conditions for both the SCHEX and the PCHEX. It should be noted that the main reason for choosing the materials of CHEXs in the experimental part of this study was to validate the model for different range of thermal conductivities with two orders of magnitude difference (SCHEX and PCHEX with tube thermal conductivities of 14.7 W/m·K and 0.33 W/m·K, respectively). It should be noted that the thermal conductivity of the FEP tubes was measured in our lab using a custom-made GHF device, as per ASTM Standard E1530-11 [45] .Figure 3-13 shows the predicted total heat transfer rate and heat recovery efficiency vs. measured values. It should be noted that the data of these figures include both SCHEX and PCHEX. As shown in Figure 3-13, the discrepancies between the model predictions and experimental data are within 12% for both total heat recovery rate and water recovery efficiency, within the range of inlet conditions considered in this study.

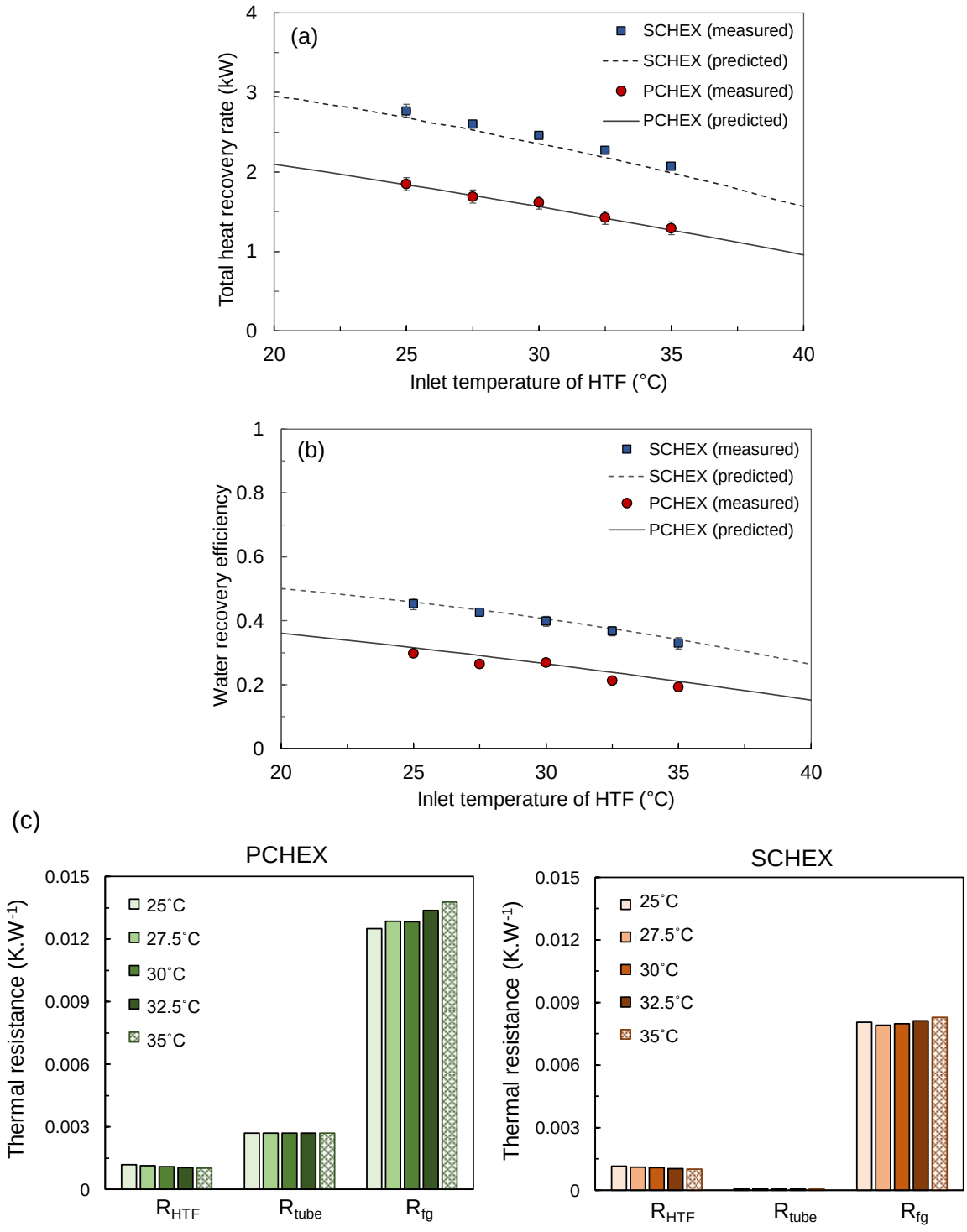

Figure 3-12. Parametric study: variation of (a) total heat recovery rate, (b) water recovery efficiency, and (c) thermal resistances of the network, shown in Figure 3-8 b, with the inlet temperature of HTF.

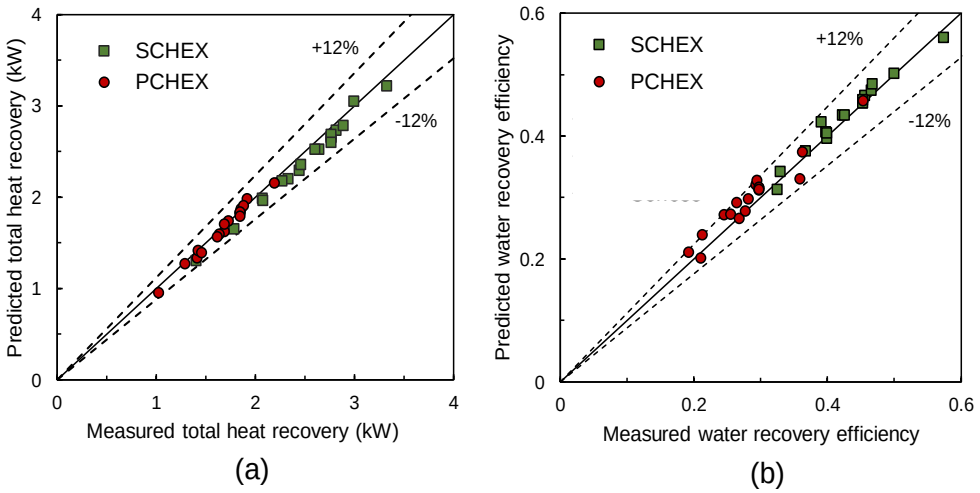

Figure 3-13. (a) Predicted vs. measured (a) total heat recovery rate and (b) water recovery efficiency.

Figure 3-14 shows the effect of inlet conditions on the HTF and flue gas pressure drops in the CHEXs. The following trends are observed:

- As expected, increasing the gas flow rate does not have any effects on the HTF pressure drop (see Figure 3-14 a).
- Increasing the flow rate of flue gas results in an increase in the flue gas pressure drop (see Figure 3-14 b). Xiong et al. [14] also reported that the flue gas pressure drop monotonously increased by increasing the velocity of the flue gas passing through the tube-bank HEX.
- Increasing the flow rate of HTF results in an increase in pressure drop in the HTF (see Figure 3-14 c).
- Although increasing the volumetric flow rate of HTF slightly increases the condensation rate, as shown in Figure 3-14 d, within the error range, increasing the volumetric flow rate of HTF flow does not have any significant effects on the gas pressure drop.
- As expected, increasing the humidity ratio of the gas flow or HTF inlet temperature does not have any effects on the HTF pressure drop (see Figure 3-14 e and g).
- As shown in Figure 3-14 f and h, within the error range, increasing the humidity ratio of the flue gas or the inlet temperature of HTF does not have any significant effect on the flue gas pressure drop, for the range of inlet conditions investigated in this study, in spite of their effects on the condensation rates.

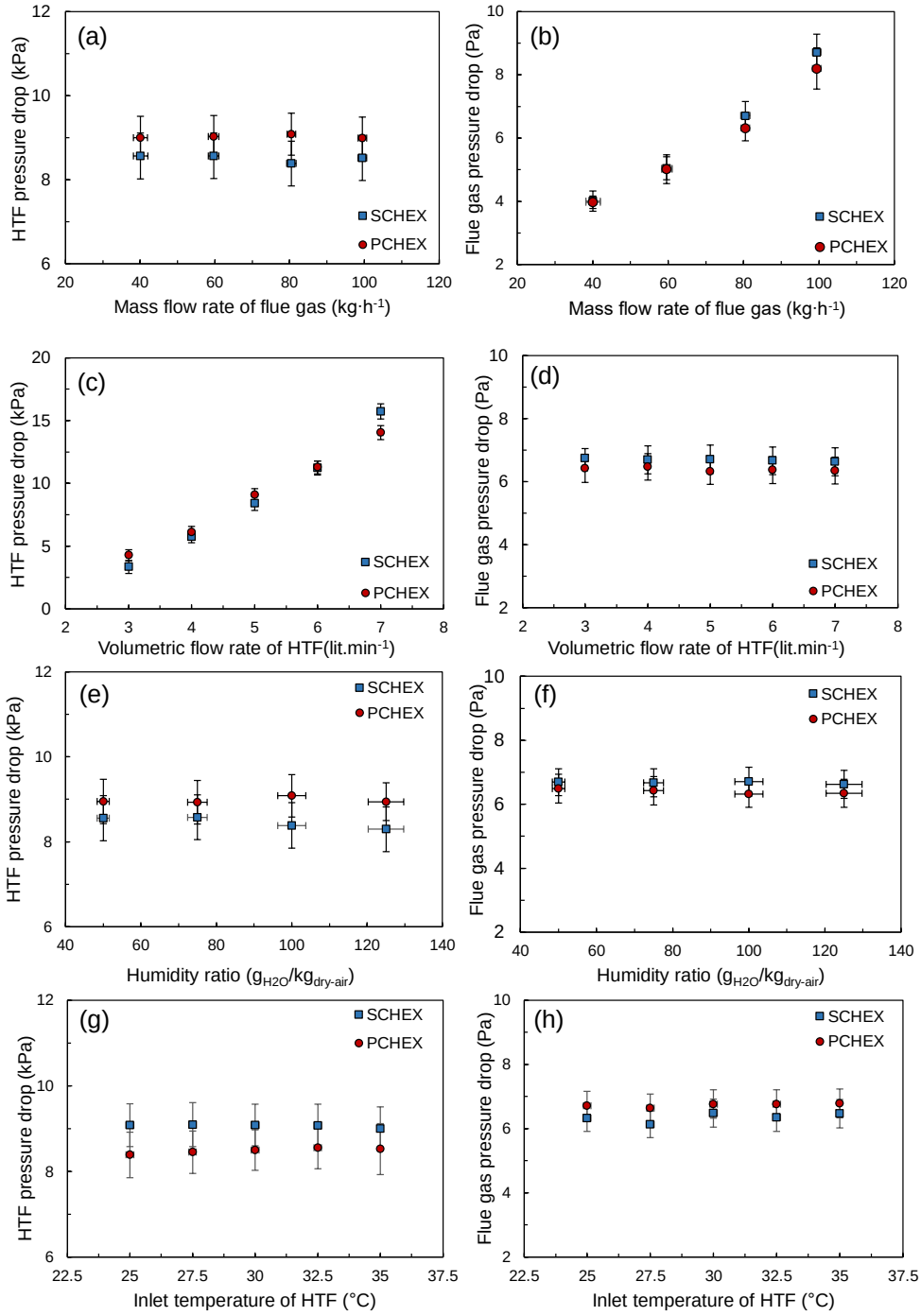

Figure 3-14. Parametric study: variation of (a, c, e, and g) HTF pressure drop and (b, d, f, and h) flue gas pressure drop in the PCHEX and SCHEX with (a and b) mass flow rate of flue gas; (c and d) volumetric flow rate of the HTF; (e and f) humidity ratio of the flue gas; and (a and b) HTF Inlet temperature.

3.6. Role of heat exchanger's material in the performance of a CHEX

To reduce the capital cost of HWRUs, it is crucial to choose the material for a CHEX in a way to reach the maximum heat and water recovery efficiency with minimum material and fabrication costs. Therefore, it is essential to investigate the significance of thermal conductivity of the material of tubes in the heat and water recovery efficiency of a CHEX. For this purpose, the analytical model, developed and validated in this study, was used to predict the performance of CHEXs made of materials with different thermal conductivities, with the same size, geometry, and inlet conditions. The variation of the total heat recovery rate and the water recovery efficiency with the thermal conductivity of CHEX's material are shown in Figure 3-15 to Figure 3-18 for different inlet conditions. These modeling results show that increasing the thermal conductivity of the tubes up to a threshold significantly enhances the efficiency of a CHEX. However, increasing the thermal conductivity of the tubes more than a threshold does not have any significant effects on the heat recovery rate and water recovery efficiency of the CHEX. As shown in Figure 3-15 to Figure 3-18, although the same trend is observed for all inlet conditions considered in this study, changing the inlet conditions slightly affects the thermal conductivity threshold. In order to further quantify the results of these figures, three different thresholds are defined in this study as follows:

- $\lambda_{0.8}$: thermal conductivity threshold to reach 80 percent of the efficiency of the same CHEX made of stainless steel
- $\lambda_{0.9}$: thermal conductivity threshold to reach 90 percent of the efficiency of the same CHEX made of stainless steel
- $\lambda_{0.95}$: thermal conductivity threshold to reach 95 percent of the efficiency of the same CHEX made of stainless steel

Thermal conductivity thresholds to reach 80, 90, and 95 percent of a CHEX with the same size and geometry made of stainless steel for different inlet conditions are listed in Table 3.6.

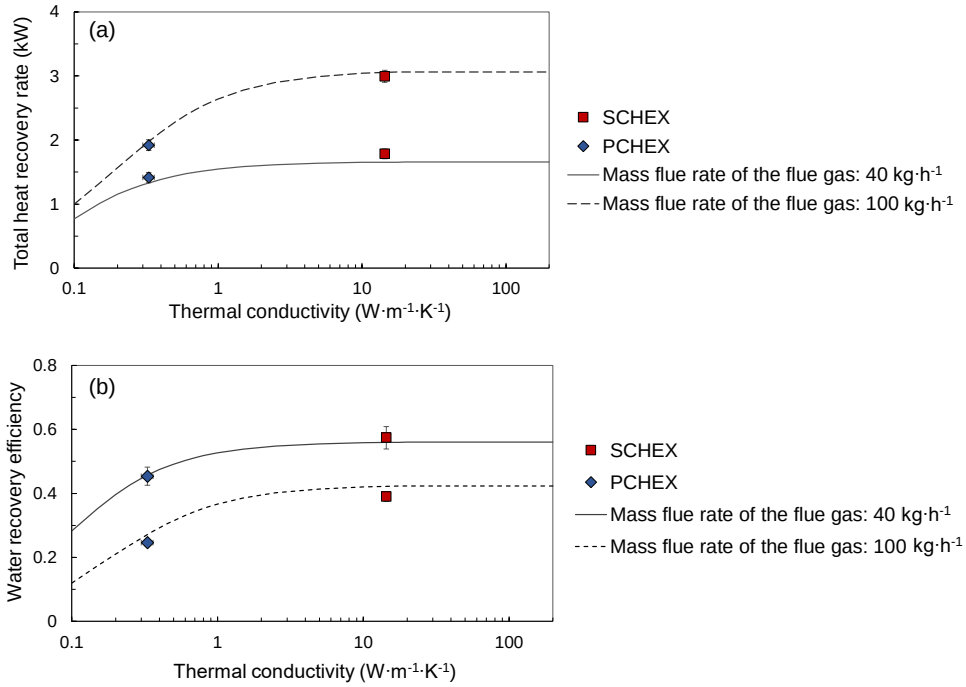

Figure 3-15. Variation of (a) total heat recovery rate and (b) water recovery efficiency of a CHEX with thermal conductivity (Inlet conditions are the same as the baseline case listed in Table 3.5 except for the mass flow rate of the flue gas).

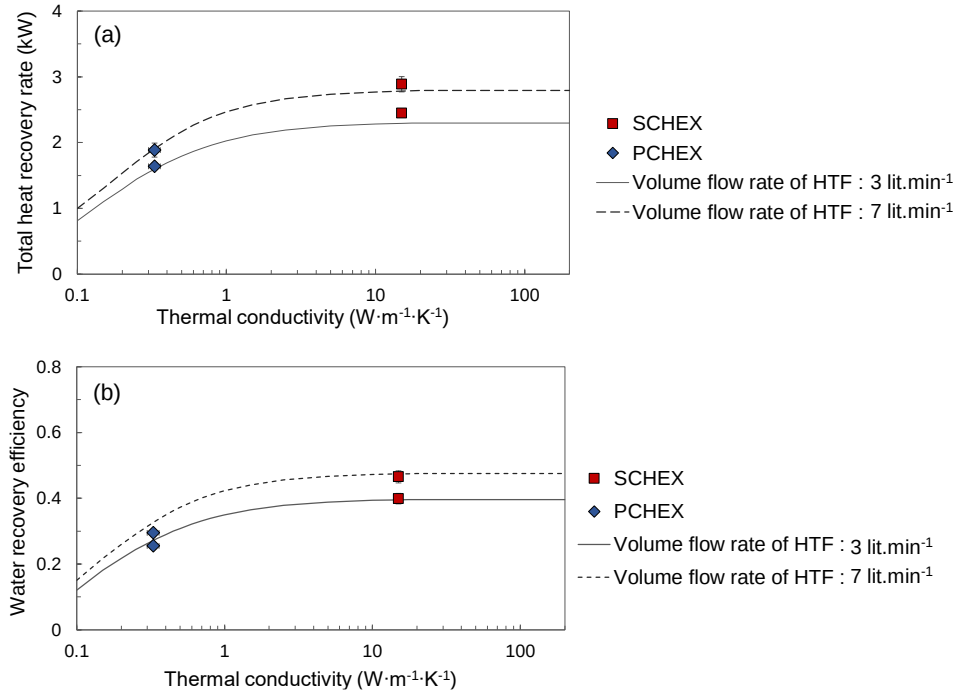

Figure 3-16. Variation of (a) total heat recovery rate and (b) water recovery efficiency of a CHEX with thermal conductivity (Inlet conditions are the same as the baseline case listed in Table 3.5 except for the volume flow rate of the HTF).

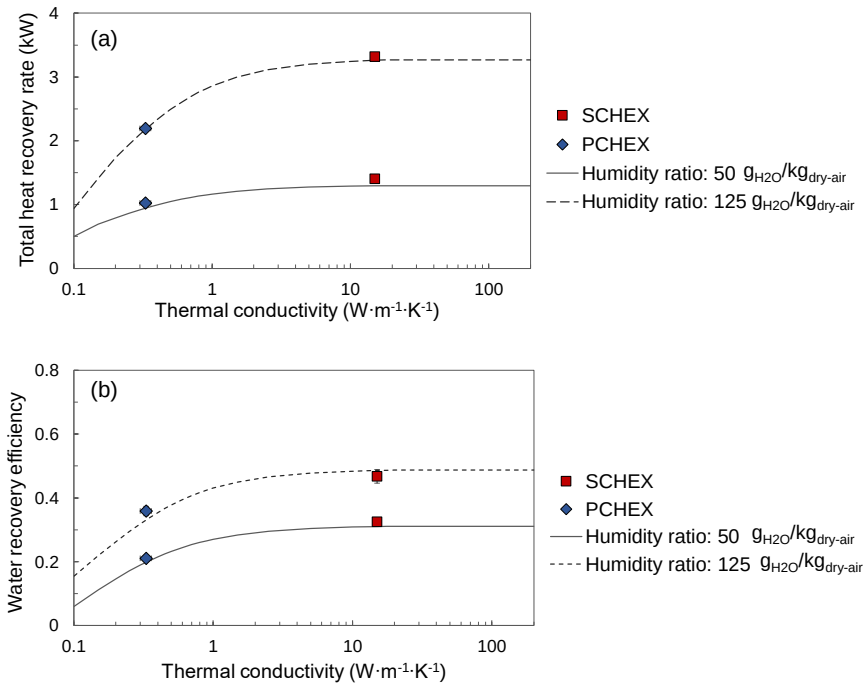

Figure 3-17. Variation of (a) total heat recovery rate and (b) water recovery efficiency of a CHEX with thermal conductivity (Inlet conditions are the same as the baseline case listed in Table 3.5 except for the humidity ratio of flue gas).

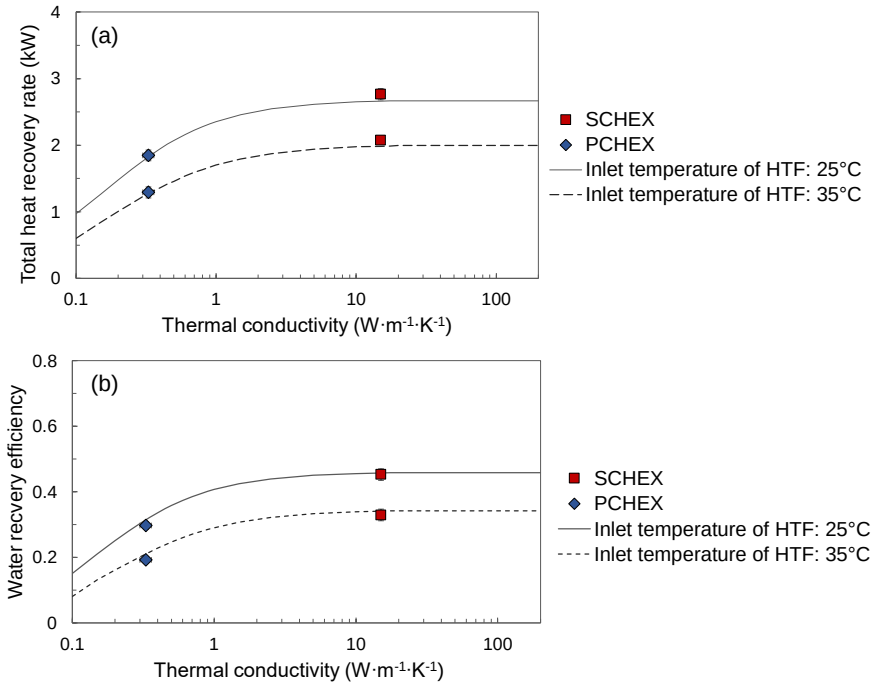

Figure 3-18. Variation of (a) total heat recovery rate and (b) water recovery efficiency of a CHEX with thermal conductivity (Inlet conditions are the same as the baseline case listed in Table 3.5 except for the HTF inlet temperature).

Table 3.6. Thermal conductivity thresholds of a CHEX's material to reach 80% ($\lambda_{0.8}$), 90% ($\lambda_{0.9}$), and 95% ($\lambda_{0.95}$) of total heat recovery rate and water recovery efficiency of a CHEX with the same geometry and inlet conditions made of stainless steel (Inlet conditions are the same as the baseline case listed in Table 3.5 except for parameters listed in the table).

Inlet conditions		Total heat recovery rate			Water recovery efficiency		
		$\lambda_{0.8}$ (W/m·K)	$\lambda_{0.9}$ (W/m·K)	$\lambda_{0.95}$ (W/m·K)	$\lambda_{0.8}$ (W/m·K)	$\lambda_{0.9}$ (W/m·K)	$\lambda_{0.95}$ (W/m·K)
Humidity ratio of the flue gas ($g_{H2O}/kg_{dry\text{-}air}$)	50	0.5	1	1.9	0.7	1.3	2.4
	75	0.6	1.1	2.1	0.6	1.2	2.1
	100	0.6	1.2	2.2	0.6	1.1	2.1
	125	0.6	1.2	2.3	0.6	1.1	2.1
Inlet temperature of the HTF (°C)	25	0.6	1.2	2.2	0.6	1.1	2.1
	27.5	0.6	1.2	2.3	0.6	1.2	2.3
	30	0.7	1.2	2.4	0.7	1.3	2.4
	32.5	0.7	1.4	2.7	0.7	1.4	2.5
	35	0.7	1.5	3	0.7	1.5	2.8
Volume flow rate of the HTF ($lit.min^{-1}$)	3	0.6	1.2	2.5	0.6	1.2	2.5
	4	0.6	1.2	2.3	0.6	1.2	2.1
	5	0.6	1.2	2.2	0.6	1.1	2.1
	6	0.6	1.2	2.1	0.6	1.1	2.1
	7	0.6	1.2	2	0.6	1.1	2
Mass flow rate of the flue gas ($kg{\cdot}h^{-1}$)	40	0.4	0.7	1.5	0.4	0.7	1.2
	60	0.5	1	1.9	0.5	0.9	1.7
	80	0.6	1.2	2.2	0.6	1.1	2.1
	100	0.7	1.5	2.6	0.7	1.3	2.5

Chapter 4.

Conclusions and future work

An analytical model was developed in this study to predict the performance of CHEXs as the core components of HWRUs. The model included the thermal conductivity of the CHEX's material as one of its inputs. Moreover, a custom-built HWRU with replaceable tubes was designed to measure the effect of tubes' material on heat and water recovery efficiency of HWRUs. In a comprehensive parametric study, the modeling results were compared with the experimental data for HWRUs made of stainless steel and FEP plastic tubes, under various inlet conditions. Moreover, the thermal resistance network of heat and water recovery in a CHEX was investigated in detail for different inlet conditions to shed light on the dominant resistance of this network. The results showed that although R_{HTF} and R_{tube} were much lower than R_{fg}, they had significant effects on the efficiency of the system. The main reason behind these observations was that an increase in the summation of R_{HTF} and R_{tube} resulted in an increase in the interface temperature, which negatively affected the condensation rate and the total heat recovery rate. It should be noted that the resistance between the flue gas and the outer surface of the tube is dominant in the resistance network. The results of the parametric study showed that increasing the humidity ratio or mass flow rate of the flue gas decreased the thermal resistance of the gas side and therefore led to a significant increase in heat and water recovery rates. However, increasing the HTF flow rate decreased the convective thermal resistance inside the tubes (R_{HTF}) but led to a much less enhancement in the heat and water recovery rates. The results also showed that increasing the temperature of the HTF flow significantly deteriorated the heat and water recovery rates. The main reason behind this observation was increasing the interface temperature as a result of increasing the inlet temperature of the HTF flow.

The effect of the material's thermal conductivity on the performance of a CHEX was investigated using the analytical model, which was developed and validated in this study. The results showed that increasing the thermal conductivity of the material, up to a threshold, significantly enhanced the performance of the unit. However, any further increase in the thermal conductivity after this threshold led only to marginal improvements. The parametric study showed that the threshold slightly changed by changing the inlet

conditions. The threshold of thermal conductivity to reach 95 percent of the performance of the same unit made of stainless steel was lower than 3 $W \cdot m^{-1} \cdot K^{-1}$ for the range of inlet conditions considered in this study. These results showed that plastics and polymers with thermally conductive additives were promising candidates to be used as the material of HWRUs. The potential directions for future work on this study are as follows:

- Investigating the effect of layout, sizing and orientation of a CHEX's tubes on the performance of the unit
- Improving the analytical model by including the effect of other material properties such as surface properties and mechanical properties
- Designing, building, and testing a pilot-scale HWRU made of plastic with thermally conductive additives to recover heat and water from the actual boiler 's flue gas
- Investigating the impact of the flue gas pressure on the heat and water recovery from both modeling and experimental point of views

References

[1] H.-W. Schiffer, T. Kober, and E. Panos, “World Energy Council’s Global Energy Scenarios to 2060,” *Zeitschrift für Energiewirtschaft*, vol. 42, no. 2, pp. 91–102, 2018.

[2] “Commercial and industrial innovation | Natural Resources Canada.” [Online]. Available: http://www.nrcan.gc.ca/energy/efficiency/industry/processes/5493. [Accessed: 31-May-2018].

[3] “Industrial Energy Systems | Natural Resources Canada.” [Online]. Available: http://www.nrcan.gc.ca/energy/efficiency/industry/processes/energy-systems/5607. [Accessed: 31-May-2018].

[4] B. P. E. Outlook, “BP Energy Outlook – 2019 Insights from the Evolving transition scenario – China BP Energy Outlook

[5] H. Lu, L. Price, and Q. Zhang, “Capturing the invisible resource: Analysis of waste heat potential in Chinese industry,” *Appl. Energy*, vol. 161, no. 2016, pp. 497–511, 2016.

[6] F. D. Dockrill, P., & Friedrich, “Boilers and heaters: improving energy efficiency,” *Nat. Resour. Canada, Off. Energy Effic.*, 2001.

[7] A. Bahadori, “Estimation of combustion flue gas acid dew point during heat recovery and efficiency gain,” *Applied Thermal Engineering*, vol. 31, no. 8–9. pp. 1457–1462, 2011.

[8] R. E. Sonntag, C. Borgnakke, G. J. Van Wylen, and S. Van Wyk, *Fundamentals of thermodynamics*, vol. 6. Wiley New York, 1998.

[9] E. Levy, H. Bilirgen, K. Jeong, M. Kessen, C. Samuelson, and C. Whitcombe, “Recovery of water from boiler flue gas,” 2008.

[10] K. Comakli, “Economic and environmental comparison of natural gas fired conventional and condensing combi boilers,” *J. Energy Inst.*, vol. 81, no. 4, pp. 242–246, 2008.

[11] D. Che, Y. Liu, and C. Gao, “Evaluation of retrofitting a conventional natural gas fired boiler into a condensing boiler,” *Energy Convers. Manag.*, vol. 45, no. 20, pp. 3251–3266, 2004.

[12] Y. Qin, H. Fu, J. Wang, M. Liu, and J. Yan, “Waste heat and water recovery characteristics of heat exchangers for dryer exhaust,” *Dry. Technol.*, vol. 36, no. 6, pp. 709–722, 2018.

[13] P. Szulc, T. Tietze, and K. Wójs, “Studies on the process of recovering low-

temperature waste heat from a flue gas in a pilot-scale plant," *Chem. Process Eng.*, vol. 37, no. 4, pp. 529–543, 2016.

[14] Y. Xiong, H. Tan, Y. Wang, W. Xu, H. Mikulčić, and N. Duić, "Pilot-scale study on water and latent heat recovery from flue gas using fluorine plastic heat exchangers," *J. Clean. Prod.*, vol. 161, pp. 1416–1422, 2017.

[15] L. Jia, X. Li, J. Sun, and X. Peng, "An experimental study on latent heat recovery of exhaust wet flue gas," *J. Therm. Sci.*, vol. 11, no. 2, pp. 144–147, 2002.

[16] K. Hwang, C. ho Song, K. Saito, and S. Kawai, "Experimental study on titanium heat exchanger used in a gas fired water heater for latent heat recovery," *Appl. Therm. Eng.*, vol. 30, no. 17–18, pp. 2730–2737, 2010.

[17] X. Zhao, L. Fu, W. Yuan, F. Li, and Q. Li, "The Potential and Approach of Flue Gas Waste Heat Utilization of Natural Gas for Space Heating," *Procedia Eng.*, vol. 146, pp. 494–503, 2016.

[18] M. Terhan and K. Comakli, "Design and economic analysis of a flue gas condenser to recover latent heat from exhaust flue gas," *Appl. Therm. Eng.*, vol. 100, pp. 1007–1015, 2016.

[19] Y. Xiong, Y. Niu, X. Wang, and H. Tan, "Pilot study on in-depth water saving and heat recovery from tail flue gas in lignite-fired power plant," *Energy Procedia*, vol. 61, pp. 2558–2561, 2014.

[20] Y. Li *et al.*, "Method of flash evaporation and condensation - heat pump for deep cooling of coal-fired power plant flue gas: Latent heat and water recovery," *Appl. Energy*, vol. 172, pp. 107–117, 2016.

[21] K. Jeong, M. J. Kessen, H. Bilirgen, and E. K. Levy, "Analytical modeling of water condensation in condensing heat exchanger," *Int. J. Heat Mass Transf.*, vol. 53, no. 11–12, pp. 2361–2368, 2010.

[22] S. Irmak, "Challenges of Biomass Utilization for Biofuels," in *Biomass for Bioenergy-Recent Trends and Future Challenges*, IntechOpen, 2019.

[23] L. Dzurenda and A. Banski, "The Effect of Firewood Moisture Content on the Atmospheric Thermal Load by Flue Gases Emitted by a Boiler," *Sustainability*, vol. 11, no. 1, p. 284, 2019.

[24] L. Dzurenda, "3D Diagram of Heat Boiler Efficiency for Combustion of Fuelwood," *Acta Fac. Xylologiae Zvolen res Publica Slovaca*, vol. 59, no. 1, p. 149, 2017.

[25] E. S. Rubin, C. Chen, and A. B. Rao, "Cost and performance of fossil fuel power plants with CO2 capture and storage," *Energy Policy*, vol. 35, no. 9, pp. 4444–4454, 2007.

[26] J. Uotila, “HEAT RECOVERY AND ENVIRONMENTAL IMPACTS OF FLUE GAS CONDENSING,” Aalto University, 2015.

[27] L. Jia, X. Li, J. Sun, and X. Peng, “An experimental study on latent heat recovery of exhaust wet flue gas,” *J. Therm. Sci.*, vol. 11, no. 2, pp. 144–147, 2002.

[28] E. Levy, H. Bilirgen, and J. Dupont, “Recovery of Water From Boiler Flue Gas Using Condensing Heat Exchangers,” *DOE Rep.*, no. DE-NT0005648, 2011.

[29] P. Stehlík, “Conventional versus specific types of heat exchangers in the case of polluted flue gas as the process fluid - A review,” *Appl. Therm. Eng.*, vol. 31, no. 1, pp. 1–13, 2011.

[30] H. M. Liu, M. Q. Chen, and L. Jia, “Condensation characteristics of flue gas/steam mixtures with fine lignite and ash particles along horizontal finned tube bundles,” *Exp. Heat Transf.*, vol. 28, no. 6, pp. 580–592, 2015.

[31] S. K. Hong, S. Park, S.-Y. Jeon, and K.-S. Lee, “Experimental study on heat transfer characteristics of water-spray-bed heat exchanger,” *J. Mech. Sci. Technol.*, vol. 29, no. 5, pp. 2243–2247, 2015.

[32] J. Mihara, T. Itoh, S. Horiki, and M. Osakabe, “Compact heat exchanger for latent heat recovery of exhaust flue gas.,” *Int. J. Heat Exch.*, vol. 4, pp. 109–126, 2003.

[33] X. Shi, D. Che, B. Agnew, and J. Gao, “An investigation of the performance of compact heat exchanger for latent heat recovery from exhaust flue gases,” *Int. J. Heat Mass Transf.*, vol. 54, no. 1–3, pp. 606–615, 2011.

[34] A. Macháčková, R. Kocich, M. Bojko, L. Kunčická, and K. Polko, “Numerical and experimental investigation of flue gases heat recovery via condensing heat exchanger,” *Int. J. Heat Mass Transf.*, vol. 124, pp. 1321–1333, 2018.

[35] L. Jia, X. F. Peng, J. D. Sun, and T. B. Chen, “An experimental study on vapor condensation of wet flue gas in a plastic heat exchanger,” *Heat Transf. Res. Co-sponsored by Soc. Chem. Eng. Japan Heat Transf. Div. ASME*, vol. 30, no. 7, pp. 571–580, 2001.

[36] H. A. Navarro and L. Cabezas-Gomez, “A new approach for thermal performance calculation of cross-flow heat exchangers,” *Int. J. Heat Mass Transf.*, vol. 48, no. 18, pp. 3880–3888, 2005.

[37] S. Zhang, X. Cheng, and F. Shen, “Condensation Heat Transfer with Non-Condensable Gas on a Vertical Tube,” *Energy Power Eng.*, vol. 10, no. 04, p. 25, 2018.

[38] V. Gnielinski, “New equations for heat and mass transfer in turbulent pipe and channel flow,” *Int. Chem. Eng.*, vol. 16, no. 2, pp. 359–368, 1976.

[39] F. P. Incropera, A. S. Lavine, T. L. Bergman, and D. P. DeWitt, *Fundamentals of heat and mass transfer*. Wiley, 2007.

[40] A. Žukauskas, “Heat transfer from tubes in crossflow,” in *Advances in heat transfer*, vol. 8, Elsevier, 1972, pp. 93–160.

[41] G. W. Thomson, “The Antoine equation for vapor-pressure data,” *Chem. Rev.*, vol. 38, no. 1, pp. 1–39, 1946.

[42] T. J. Ypma, “Historical development of the Newton--Raphson method,” *SIAM Rev.*, vol. 37, no. 4, pp. 531–551, 1995.

[43] E. N. ISO, “5167: Measurement of Fluid Flow by means of Pressure Differential Devices,” *Int. Organ. Stand. Genève*, 2003.

[44] R. J. Moffat, “Contributions to the theory of single-sample uncertainty analysis,” *J. Fluids Eng.*, vol. 104, no. 2, pp. 250–258, 1982.

[45] E.-11 ASTM, “Standard test method for evaluating the resistance to thermal transmission of materials by the guarded heat flow meter technique.” ASTM International West Conshohocken, PA, 2011.

Appendix A.

Heat recovery efficiency

As mentioned before, since the share of sensible heat recovery is much less than the latent heat recovery, the value of heat recovery efficiency of a CHEX is close to its water recovery efficiency. Figure A1 compares the heat and water recovery efficiency of both SCHEX and PCHEX for different inlet conditions which proves this point. The maximum difference between energy recovery efficiency and heat recovery efficiency is 2.7%.

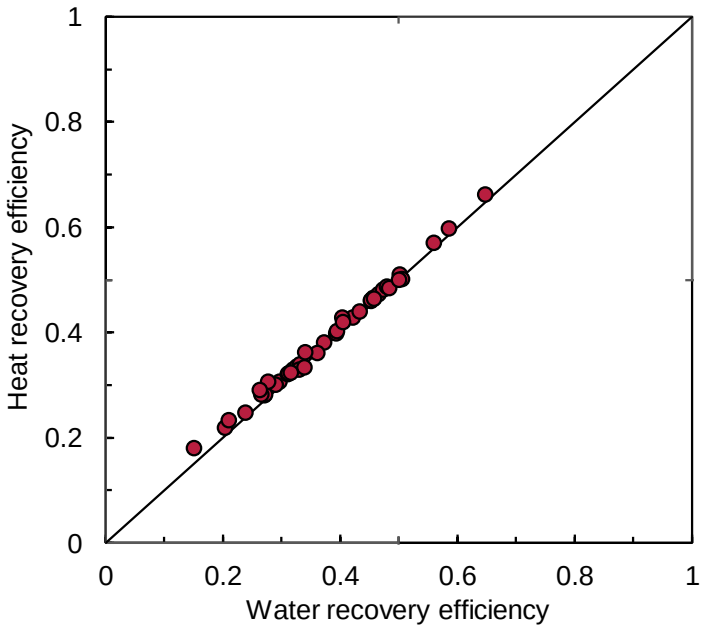

Figure A1. Heat recovery efficiency vs. water recovery efficiency of the SCHEX and the PCHEX; inlet mass flue rate of the flue gas: 40-100 kg.h^{-1}; inlet flue gas temperature: 70°C, inlet gas humidity ratio: 50-125 $g_{H2O}/kg_{dry-air}$, inlet HTF temperature: 25-35°C, and HTF volume flow rate: 3-7 lit.min^{-1}).

Appendix B.

Uncertainty analysis

The main formulas for calculating the uncertainty of different parameters are listed in Table B1[44].

Table B1. Summary of basic formulas for the uncertainty calculations

$R_1 = R_1(x_1, x_2, \dots, x_n)$	$\delta(R_1) = \left\{\left(\frac{\partial R_1}{\partial x_1}\delta x_1\right)^2 + \left(\frac{\partial R_1}{\partial x_2}\delta x_2\right)^2 + \cdots + \left(\frac{\partial R_1}{\partial x_n}\delta x_n\right)^2\right\}^{1/2}$
$R_2 = x_1^a x_2^b \dots x_n^i$	$\frac{\delta(R_2)}{R_2} = \left\{\left(a\frac{\delta x_1}{x_1}\right)^2 + \left(b\frac{\delta x_2}{x_2}\right)^2 + \cdots + \left(i\frac{\delta x_n}{x_n}\right)^2\right\}^{1/2}$
$R_3 = x_1 + x_2 + \cdots + x_n$	$\delta(R_3) = \{(\delta x_1)^2 + (\delta x_2)^2 + \cdots + (\delta x_n)^2\}^{1/2}$